INVESTIGATION OF AERODYNAMIC EFFECTS ON PERFORMANCE OF WIND TURBINE BLADES BY USING FINITE ELEMENT METHOD

A Thesis Submitted To
the Graduate School of Engineering and Sciences of
İzmir Institute of Technology
in Partial Fulfillment of the Requirements for the Degree of

MASTER OF SCIENCE

in Energy Engineering

by
Mehmet Mahir TOSUN

July 2005
İZMİR

We approve the thesis of **Mehmet Mahir TOSUN**

Date of Signature

……
Assoc. Prof. Dr. Barış ÖZERDEM **26 July 2005**
Supervisor
Department of Mechanical Engineering
İzmir Institute of Technology

……
Assoc. Prof. Dr. Metin TANOĞLU **26 July 2005**
Co-Supervisor
Department of Mechanical Engineering
İzmir Institute of Technology

……
Prof. Dr. Zafer İLKEN **26 July 2005**
Department of Mechanical Engineering
İzmir Institute of Technology

……
Asst. Prof. Dr. Dilek KUMLUTAŞ **26 July 2005**
Department of Mechanical Engineering
Dokuz Eylül University

……
Asst. Prof. Dr. Gülden GÖKÇEN **26 July 2005**
Head of Department of Energy Engineering
İzmir Institute of Technology

……
Assoc. Prof. Dr. Semahat ÖZDEMİR
Head of the Graduate School

ACKNOWLEDGMENTS

I would like to express my sincere gratitude to my supervisor, Assoc.Prof.Dr. Barış Özerdem, for his instructive comments, valuable guidance and continual support throughout the steps of this study.

I also wish to thank my friend Levent Bilir for his friendship and supports.

Finally, special thanks to my wife for her encouragement and support during my study.

ABSTRACT

In this study, design of the most suitable wind turbine rotor for Iztech campus area is performed by taking into account aerodynamic effects.

Aerodynamic properties of various airfoils are determined, numerically, by using a software called FLUENT. Blade element momentum theory is applied to find chord lengths and twist angles for mean wind speed at 10m height in Iztech campus area. Rotor performance is determined by using blade element momentum theory. Effects of twist angle and tip speed ratio are investigated for blade design. Rotor maximum power coefficient of the new designed blade is found as 0.4313 while another design in use gives a maximum power coefficient of 0.4044.

It can be noted that new designed blade is more efficient, as it gives the maximum power coefficient at design conditions, 6.85 m/s wind speed at 10 m height and 25^{o}C ambient temperature. It is observed that new design gives higher power values than the design in use, over 5.8 m/s wind speed.

ÖZET

Bu çalışmada, İYTE kampüs alanı için en uygun rüzgar türbini rotor tasarımı aerodinamik etkiler göz önüne alınarak gerçekleştirilmiştir.

Çeşitli kanat profillerinin aerodinamik özellikleri, sayısal olarak, FLUENT adlı bir yazılımın kullanımıyla belirlenmiştir. İYTE kampüs alanında ölçülen 10 m yükseklikteki ortalama hız değeri için veter kalınlıkları ve burulma açıları kanat elemanı momentum teorisi uygulanarak hesaplanmıştır. Kanat tasarımında burulma açıları ve uç hız oranlarının etkileri incelenmiştir. Rotor performansının bulunması için kanat elemanı momentum teorisi kullanılmıştır. Yeni tasarlanan rotor kanadının en yüksek güç katsayısı 0.4313 iken kullanılmakta olan başka bir tasarımın en yüksek güç katsayısı 0.4044 olarak bulunmuştur.

Yeni kanat tasarımının 10m yükseklikte 6.85 m/s rüzgar hızı ve 25^{o}C çevre sıcaklığı tasarım koşullarında en yüksek güç katsayısını vermesi nedeniyle yeni kanat tasarımının daha verimli olduğu görülmüştür. Yeni kanat tasarımının kullanılmakta olan diğer tasarıma göre 5.8 m/s rüzgar hızından sonraki değerlerde daha yüksek güç değerlerine ulaştığı gözlemlenmiştir.

TABLE OF CONTENTS

LIST OF FIGURES

Figure **Page**

LIST OF TABLES

Table **Page**

LIST OF SYMBOLS

A	Cross- sectional area of stream, (m^2)
a	Axial induction factor
a'	Angular induction factor
α	Empirical wind shear exponent
AR	Aspect ratio.Span length divided by chord width
α_{stall}	Attack angle at stall, (8degree)
B	Blade number
BEM	Blade element momentum
C	Chord length, (m)
C_D	Drag coefficient. Ratio of the drag force to the dynamic pressure for unit span area, $D/(\rho V^2 A)$.
$C_{D\ stall}$	Drag coefficient at stall
C_L	Lift coefficient. Ratio of the lift force to the dynamic pressure for unit span area, $L/(\rho V^2 A)$.
$C_{L\ stall}$	Lift coefficient at stall
C_p	Power coefficient
$C_{p,rat}$	Rated power coefficient
D	Drag force, (N)
dr	Annulus width, (m)
Φ	Inflow angle,(degree)
F	Correction factor
F_{Hub}	Hub correction factor
F_{Tip}	Tip correction factor
F_{Total}	Total correction factor
H_0	Surface roughness length, (m)
L	Lift force, (N)
λ	Tip speed ratio
λ_r	Local tip speed ratio
ν	Kinematic viscosity of air (m^2/s)
NACA	National Advisory Committee for Aeronautics
P_D	Power calculated by actuator disc theory, (Watt)
PFC	Power factor correction
P_{rat}	Rated power, (Watt)
P_{tot}	Total power, (Watt)
P_W	Power calculated by energy theory, (Watt)
P_{w0}	Power in free stream wind, (Watt)
Q	Torque, (N.m)

r	Radial position, (m)
ρ	Incoming wind density, (kg/m^3)
rpm	Revolution per minute
T	Thrust, (N)
U	Wind speed at rotor surface, (m/s)
V_2	Far stream wind velocity, (m/s)
V_a	Wind speed at height "a", (m/s)
V_b	Wind speed at height "b", (m/s)
V_{total}	Local velocity component, (m/s)
V_w	Free stream wind velocity, (m/s)
Ω	Turbine angular velocity, (rad/s)
ω	Induced angular velocity, (rad/s)
A	Angle of attack,(degree)
B	Pitch angle, (degree)
$\dot{m}$	Mass-flow rate, (kg/s)

CHAPTER 1

INTRODUCTION

A wind turbine is a device for extracting kinetic energy from the wind. It was used in ancient times as drag rotors to get higher torque to use in grind grain or water pumping but nowadays it is used to produce electricity.

The rotor is the first component of the functional units in a wind turbine. Therefore its aerodynamic properties are essential factors for the whole system in many aspects. Thus researches are mainly focused on wind turbine's aerodynamics. In 1888 Charles Brush built the first wind turbine to generate electricity with a 144 bladed wind turbine. Different designs being used are described in Chapter 3. Producing electricity needs higher rotational speeds therefore Poul LaCour designed low solidity, higher speed machines working with lift force with 4 bladed wind turbines in 1897 (WEB_1 2005).

Wind turbine's power approach has been done in 1922 by Betz. Later blade element momentum (BEM) theory developed by Glauert in 1935 replaced other theories as described in Chapter 4. Tip and hub loss corrections are improved by Prandtl for BEM theory (Shepherd 1998).

For maximizing rotor power coefficient several cross sections of blades (airfoils), are studied. Different airfoils designed for airplane wings, propeller blades and helicopter rotors are used in wind turbine blade design. Airfoils aerodynamic properties are investigated by Abbott and Von Doenhoff in NASA (Abbott and Von Doenhoff 1959), by Fuglsang which is done at Velux (Fuglsang et. al. 1998), by Somers in Delft University (Somers 1997). New families of airfoils have been designing for wind turbine blades in Delft University, National Renewable Energy Laboratory (NREL) and Riso National Laboratory (Bak et. al., 1999). Rotor blade design is dealt with in Chapter 5.

Small mixed airfoil designed wind turbine blades have been widely used nowadays (Habali and Saleh 2000, Giguere and Selig 1999). In this study airfoil characteristics investigated with a software, as described in Chapter 6. Designed blade performance is determined by a BEM theory using a code written by Buhl which is also used by National Renewable Energy Laboratory (Buhl 2005). A new mixed airfoil blade

for a small scale wind turbine with a fixed pitch angle for Iztech campus area is designed in the present study. In order to make stall regulation and improve the performance the required design criteria such as inflow angle, twist angle and chord lengths for selected airfoils are calculated. Results of new design are compared with performance of other blade design which is used in a small scale wind turbine.

CHAPTER 2

WIND ENERGY

2.1. Wind Energy

Wind is air in motion relative to the surface of the earth. The primary cause of air motion is uneven heating of the earth by solar radiation. The air is not heated directly, but solar radiation is first absorbed by the earth's surface and is then transferred in various forms back into the overlying atmosphere. Since the surface of earth is not homogenous (land, water, desert, forest, etc.), the amount of energy that is absorbed varies both in space and time. This creates differences in atmospheric temperature, density and pressure which in turn create forces that move air from one place to another. This movement causes wind. Surface features such as mountains and valleys can change the direction and speed of prevailing winds.

Winds can be broadly classified as planetary and local. Planetary winds are caused by greater solar heating of the earth's surface near the equator than near the northern or southern poles. This causes warm tropical air to rise and flow through the upper atmosphere toward the poles and cold air from the poles to flow back to the equator nearer to the earth's surface. The direction of motion of planetary winds with respect to the earth is affected by the rotation of the earth. The western motion toward the equator and the eastern motion toward the poles result in large counterclockwise circulation of air around low-pressure areas in the northern hemisphere and clockwise circulation in the southern hemisphere (El-Wakil 1998).

Local winds are caused by two mechanisms. The first one is differential heating of water and land. Solar insolation during the day is readily converted to sensible energy of the land surface and partly consumed in evaporating some of that water. The landmass becomes hotter than the water, which causes the air above land to heat up and become warmer than the air above water. The warmer lighter air above the land rises, and the cooler heavier air above the water moves in to replace it. This is the mechanism of shore breezes. At night, the direction of the breezes is reversed because the landmass cools more rapidly than the water. Hills and mountain sides cause the second

mechanism of local winds. The air above the slopes heats up during the day and cools down at night, more rapidly than the air above the low lands. This causes heated air during the day to rise along the slopes and relatively cool heavy air to flow down at night.

Winds are very much influenced by the ground surface at altitudes up to 100 meters. The wind will be slowed down by the earth's surface roughness and obstacles. Wind speeds are affected by the friction against the surface of the earth. In general, the more pronounced the roughness of the earth's surface; the more the wind will be slowed down. Forests and large cities obviously slow the wind down considerably, while concrete runways in airports will only slow the wind down a little. Water surfaces are even smoother than concrete runways, and will have even less influence on the wind, while long grass and shrubs and bushes will slow the wind down considerably.

The roughness of the earth surface diminishes the velocity of the wind. With growing heights above ground level, the roughness has less effect and the velocity of the wind increases. Wind speed varies considerably with height above ground. This is called wind shear.

A power law is commonly used in wind engineering for defining vertical wind profiles.

$$V_b = V_a \left(\frac{h_b}{h_a} \right)^{\alpha} \tag{2.1}$$

V_b= Wind speed at height h_b

V_a= Wind speed at height h_a

α = Empirical wind shear exponent

In general the exponent α is a highly variable quantity, often changing from less than $\frac{1}{7}$ during the day to more than $\frac{1}{2}$ at night over the same terrain. In early wind energy work, it was recognized that α varies with elevation, time of day, season of the year, nature of the terrain, wind speed, temperature and various thermal and mechanical mixing parameters (Golding 1977). Spera and Richards proposed equations for α based on both the surface roughness length, h_0, and the wind speed at the reference elevation, V_a (Spera and Richards 1979). This model decreases the wind shear exponent with

increasing wind speed until the wind profile becomes vertical at a very high speed 67 m/s. For high wind speeds of short averaging times Kaufman gives (Kaufman 1977)

$$\alpha=0.55\ V_a^{-0.77} \tag{2.2}$$

Total mean wind shear value in IZTECH campus area is calculated from the collected data from June.2000 to November.2001 as 0.13 by the use of WindPro software (Ozerdem and Turkeli 2005).

2.2. Power in the Wind

Wind turbines use the kinetic energy of the wind flow. Their rotors reduce the wind velocity from the undisturbed wind speed far in front of the rotor to a reduced air stream velocity behind the rotor. The difference in wind velocity is a measure for the extracted kinetic energy which turns the rotor connected to the electrical generator.

The total power of a wind stream is equal to the rate of the incoming kinetic energy of that stream, or

$$P_{tot} = \dot{m}\frac{V_w^{\ 2}}{2} \tag{2.3}$$

where;

P_{tot}= total power, W

$\dot{m}$ = mass-flow rate, kg/s

V_w = incoming wind velocity, m/s

The mass-flow rate is given by the continuity equation

$$\dot{m} = \rho A V_w \tag{2.4}$$

where;

ρ = incoming wind density, kg/m^3

A= cross- sectional area of stream, m^2

Then equation 2.3 becomes

$$P_{tot} = \frac{1}{2}\rho A V_w^{\ 3} \tag{2.5}$$

Thus the total power of a wind stream is directly proportional to its density, area, and the cube of its velocity (Figure 2.1).

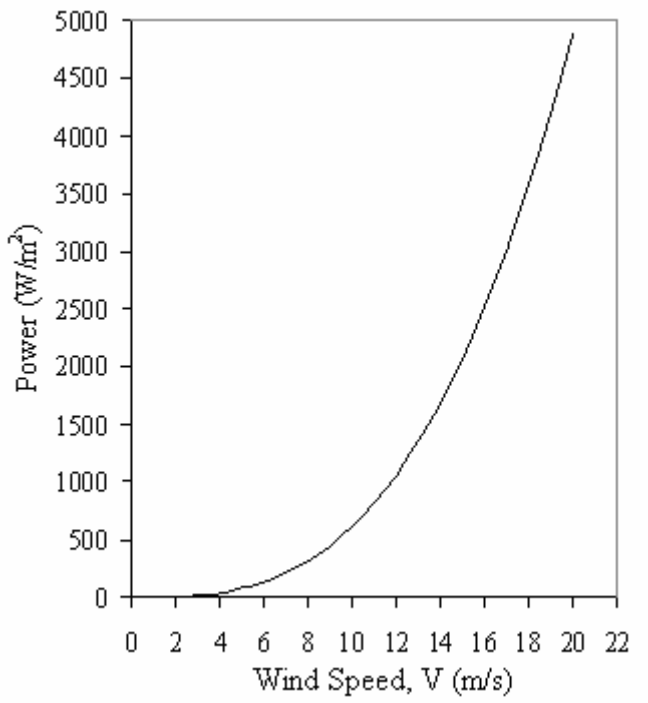

Figure 2.1. Wind power is proportional to cube of wind speed.

2.3. Global Status

World's primary energy consumption increased by 4.3% in 2004. The strongest rise was in Asia Pacific, up by 8.9%, while North America recorded the weakest growth at 1.6%. Coal remained the fastest growing fuel, rising 6.3% globally. Oil consumption grew by 3.4%, the most rapid rate since 1986. Hydroelectric and nuclear energy generations also experienced strong growth, rising 5% and 4.4%, respectively (BP 2005).

With Kyoto Protocol, a series of greenhouse gas reduction targets has cascaded down to a regional and national level. These in turn have been translated into targets for increasing the proportion of renewable energy, in the supply mix. Kyoto Protocol called for global cut of 6 % from 1990 levels by the period 2008-2012, a series of greenhouse

gas reduction targets has cascaded down to regional and national levels. Wind power and other renewable energy technologies generate electricity without producing the pollutants associated with fossil fuels and nuclear power generation, and emit no carbon dioxide, the most significant greenhouse gas.

Despite the scale of the potential, the current contribution of renewables to world energy supplies is modest. Renewables are estimated to supply around 17% of world primary energy, but most of this is from large hydroelectric schemes and the use of traditional biomass and agricultural waste in developing countries – these supply 3% (18% of electricity) and 14% of primary energy, respectively (Gross et al. 2003)

However, both can lead to considerable local environmental problems and the potential for sustainable expansion because both are limited. Meanwhile, according to IEA (International Energy Agency) the 'new' renewables such as solar, modern biomass and wind power contribute a much smaller proportion of energy needs at present – around 3% of electricity and 2% of primary energy (Hatziargyriou and Zervas 2001). Wind is the world's fastest-growing energy source, with installed generating capacity increasing by an average 32% annually for the last five years (1998-2002) (WEB_1 2005). Figure 2.2 shows the global installed wind energy capacity versus year.

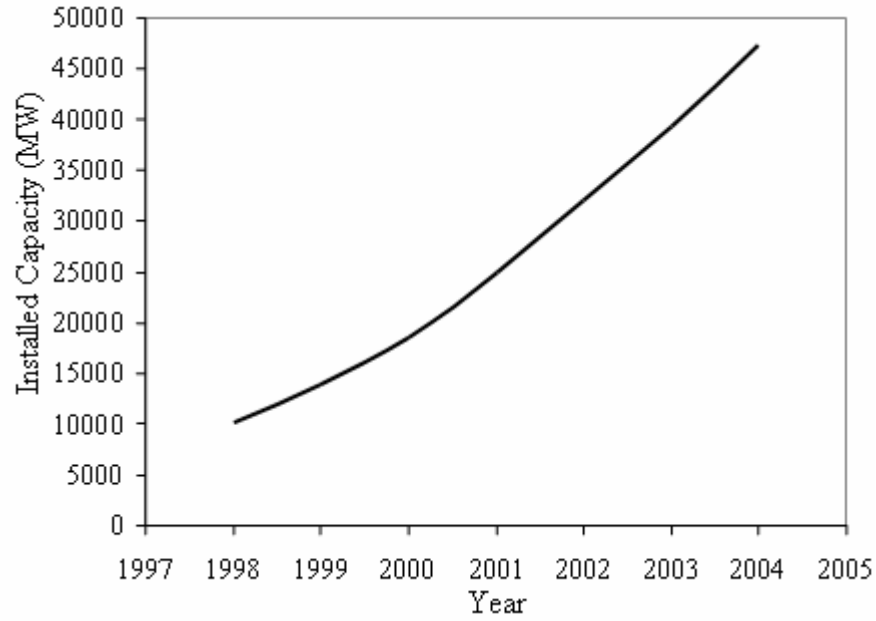

Figure 2.2. Global installed capacity of wind turbines in MW.

Total installed capacity of wind energy at the end of the 2004 is 47317 MW. Currently wind energy production represents the fastest growing of all renewable

energy sources on the market, with most of the growth coming from the Europe, (Germany, Spain and Denmark) proportions can be seen in Fig 2.3. (WEB_2 2005).

A research has been done in 2002 concluded that Turkey has a theoretical wind energy potential of nearly 90,000 MW and an economical wind energy potential of about 10,000 MW. The most promising region is in northwest Turkey (WEB_3 2005). Despite the higher wind energy potential of Turkey, the installed wind energy capacity is 20 MW at the end of the 2004. Table 2.1 gives the top wind energy markets in 2004.

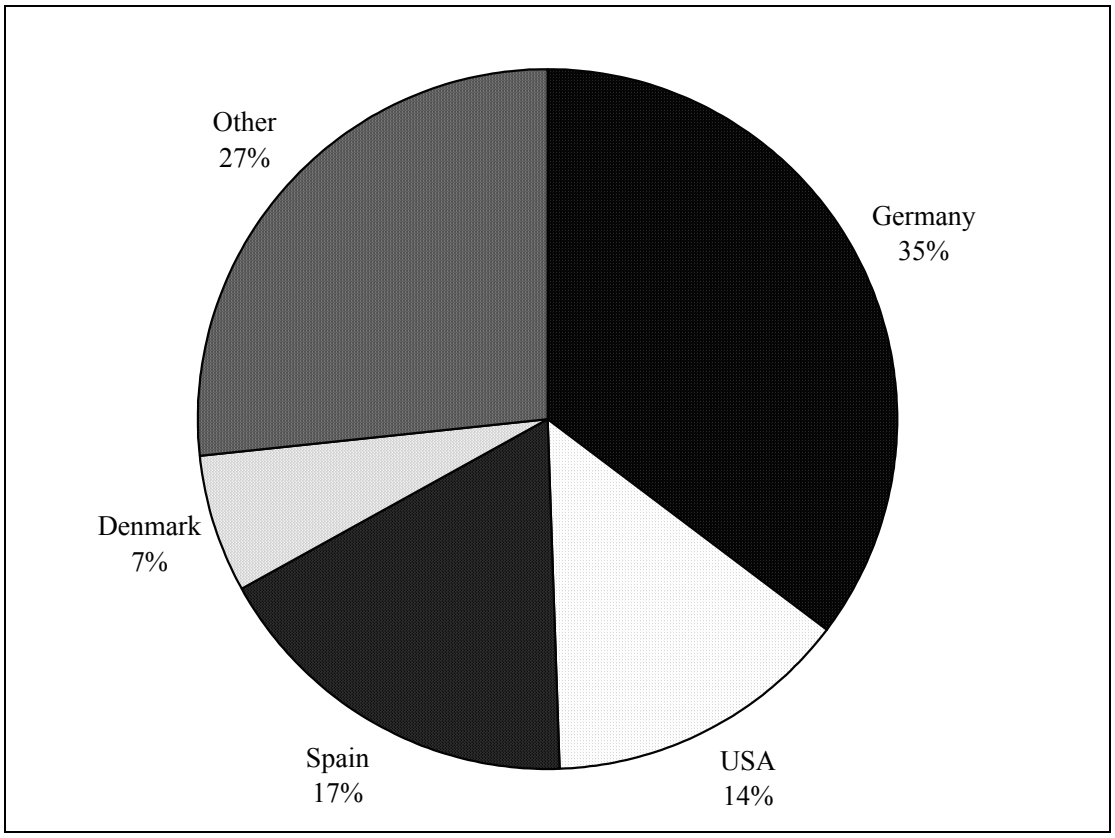

Figure 2.3. Total world wind power generation, by region at the end of 2004.

Table 2.1. Top Wind Energy Markets in 2004

(Source:WEB_2 2005).

Top Wind Energy Markets in 2004		
Country	**New Capacity in 2004 (MW)**	**Total Capacity end 2004(MW)**
Germany	2,017	16,629
USA	366	6,740
Spain	1,843	8,263
India	875	3000
Austria	192	606
Japan	275	761
Netherlands	140	1,078
Denmark	41	3,117
UK	240	888
Italy	904	1,125
Turkey	1	20
Others	268	11,156
Total World	**8,023**	**47,317**

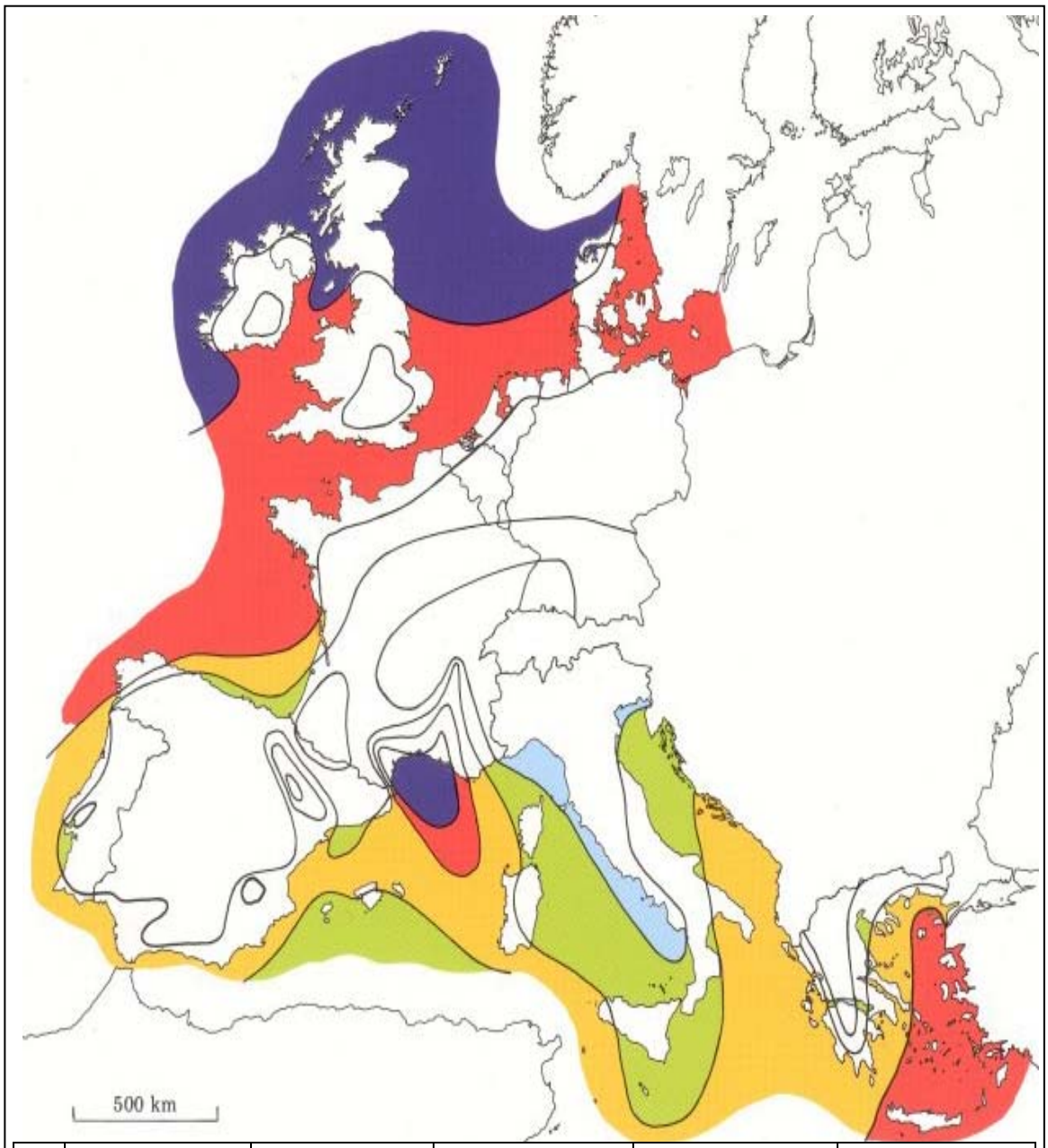

	10 m		25 m		50 m		100 m		200 m	
	m/s	W/m^2	m/s	W/m^2	m/s	W/m^2	m/s	W/m^2	m/s	W/m^2
	> 8.0	> 600	> 8.5	> 700	> 9.0	> 800	> 10.0	> 1100	> 11.0	> 1500
	7.0-8.0	350-600	7.5-8.5	450-700	8.0-9.0	600-800	8.5-10.0	650-1100	9.5-11.0	900-1500
	6.0-7.0	250-300	6.5-7.5	300-450	7.0-8.0	400-600	7.5-8.5	450-650	8.0-9.5	600-900
	4.5-6.0	100-250	5.0-6.5	150-300	5.5-7.0	200-400	6.0-7.5	250-450	6.5-8.0	300-600
	< 4.5	< 100	< 5	< 150	< 5.5	< 200	< 6.0	< 250	< 6.5	< 300

Figure 2.4. European offshore wind atlas

(Source:WEB_4 2005).

CHAPTER 3

WIND TURBINES

Wind turbines are the devices which converts the kinetic energy contained in an air stream into mechanical energy. In this chapter historical development of wind turbines, wind turbine classification and main parts of the wind turbines are introduced.

3.1. Historical Development of the Wind Turbines

The utilization of wind energy is not a new technology; it is the rediscovery of a long tradition of wind power. The first reliable information from historical sources covering the existence of wind-mills are delivered from the year 644 A.D. (Hau 2000). It tells of windmills from the Persian-Afghan border, the ancient area of Seistan (Figure 3.1.). These early windmills consist of a simple tower supporting paddles made from bundled reeds and spin the paddles around a vertical axis to grind grain. These basic types of windmills were in use in Seistan and Neh.

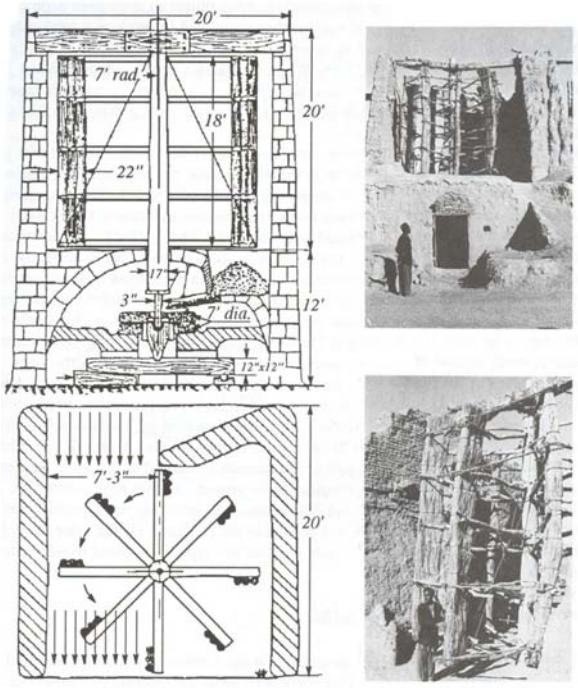

Figure 3.1. An existing windmill of the Persian type in Neh
(Source: Shepherd 1998).

In 11th century, windmills begin to be used in Europe to grind grain. Typical European windmills use four blades and turn around on a horizontal axis. In 14th century improvements are slowly made to European windmills to increase the aerodynamic lift of the blades and raise rotor speeds, allowing for superior grinding and pumping. By the late 1700s, windmills have become the "electrical motor" of pre-industrial Europe, supplying an estimated 1500 megawatts of power in Europe, a level not reached again until the late 1980s. This wind power was used for draining lands, grinding grain, milling timber and processing commodities such as spices and tobacco (WEB_5 2005).

At the end of the 19th century, interest developed in using wind power for electrical generation. At that time, it had to be direct-current (DC) power if only because of the varying speed on the windmill. In 1888, U.S. scientist and businessman Charles Brush built the first wind turbine to generate electricity in Cleveland, Ohio, it has a capacity of 12 kW of DC power for charging storage batteries on his own large estate (Shepherd 1998). The upwind rotor was a solid wheel type; with its 17 m rotor diameter and 144 blades on a tower of 18 m high (Figure 3.2.). The whole system was operated automatically. It ran for 20 years until the rotor was removed in 1908. The Brush wind turbine was a milestone, because it was the first attempt to combine the best developed structural and aerodynamic windmill technology with newly developing electrical technology. It also introduced the high step-up ratio (50:1) to wind turbine transmissions to give a full load dynamo speed of 500 rpm.

The next important step in the transition to wind turbine generators was taken by Professor Poul LaCour, in Denmark, was a scientist who put the principles of the new engineering science of aerodynamics into use in the wind turbines and he was one of the first in the world to use a wind tunnel. He appreciated the advantages of low solidity ratio, leading edge camber and low drag (Figure 3.3.) (WEB_6 2005).

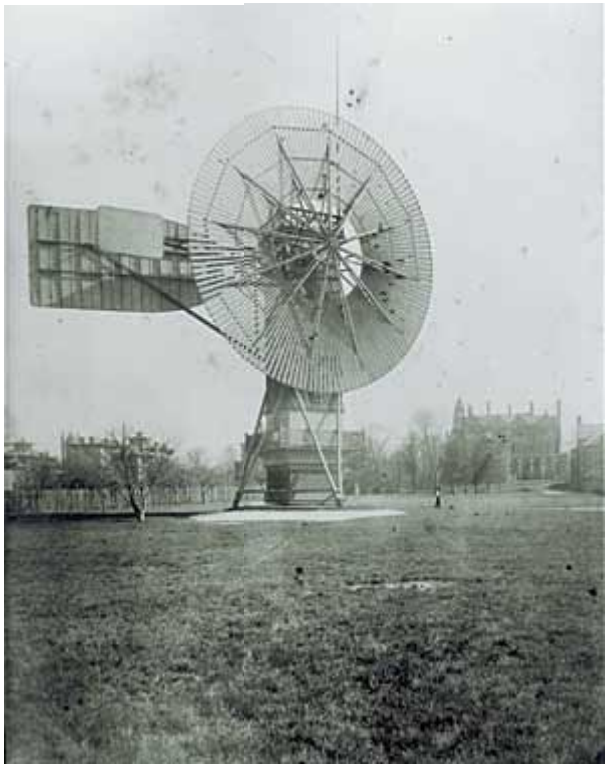

Figure 3.2. Brush's wind turbine

(Source: WEB_6 2005).

Figure 3.3.Two of LaCour's test wind turbines in 1897 at Askov Folk High School, Askov, Denmark

(Source: WEB_6 2005).

In early 1930's thousands of small wind turbines are built in rural areas across the U.S. Great Plains. One to three kilowatts in capacity, the turbines at first are installed to provide lighting for farms and to charge batteries for crystal radio sets. Later their use is extended to power appliances and farm machinery.

In late 1970s the interest in wind power generation returned as a part of response to the oil crises in 1973 and 1979. The oil crisis of 1973 caused interest in large wind turbines and encouraged government-sponsored renewable energy research programs in Germany, Sweden, Canada, Great Britain and the United States. These programs triggered the development and use of new wind turbine designs, helping to cut the cost of wind power significantly over the next two decades. Countries like Germany, USA or Sweden used this money to develop large-scale wind turbine prototypes in the MW range, others concentrated on creating the right market conditions for deployment of the technology.

Nowadays wind turbines capacities range between 600 kW to 5000 kW, and they work as a standalone or connected system to grid, by the development of aerodynamic and mechanical design parameters.

3.2. Wind Turbine Types

Wind turbines can be classified according to their aerodynamic function or their conceptual design. Whether wind energy converter captures its power exclusively from aerodynamic drag of airstream acting on rotor surfaces, or whether it is able to utilize the aerodynamic lift created by the flow against surfaces characterizes the rotor's aerodynamic function. Accordingly, they called as drag rotors and rotors which use the aerodynamic lift. Classification according to design aspects is more practicable and common. They are characterized by the position of the wind rotor's axis of rotation. Thus, they are named as rotors which have a vertical and horizontal axis of rotation.

3.2.1. Vertical Axis Machines

Wind turbines with a vertical axis of rotation represent the oldest design. Initially vertical axis rotors could only be built as pure drag rotors. Later researchers

have succeeded in developing vertical axis designs which could also effectively utilize the aerodynamic lift.

The specific advantages of vertical axis turbine concepts are, their basically simple design including the possibility of accommodating mechanical and electrical components, gear box and generator on the ground and the absence of a yaw system. This causes some disadvantages like low tip speed ratio, its inability to self start and not being able to control power output or speed by pitching the rotor blades.

The Savonius rotor, the Darrieus rotor and H rotor concepts are the main types of vertical axis machines (Figure 3.4.). The Savonius rotor can be found as ventilators or cup anemometers. The construction is simple and inexpensive. The lift solidity produces high starting torque so Savonius rotors are used for water pumping. Due to its low tip speed ratio and its comparatively low power coefficient it isn't suited for electricity generation. In the Darrieus rotor, the rotation of blades follows a spinning rope pattern, with a vertical axis of rotation which utilizes aerodynamic lift force. A variation of the Darrieus rotor is the so called H rotor. Instead of curved rotor blades, straight blades connected to the rotor shaft by struts are used. It is also known as Musgrove rotor concept.

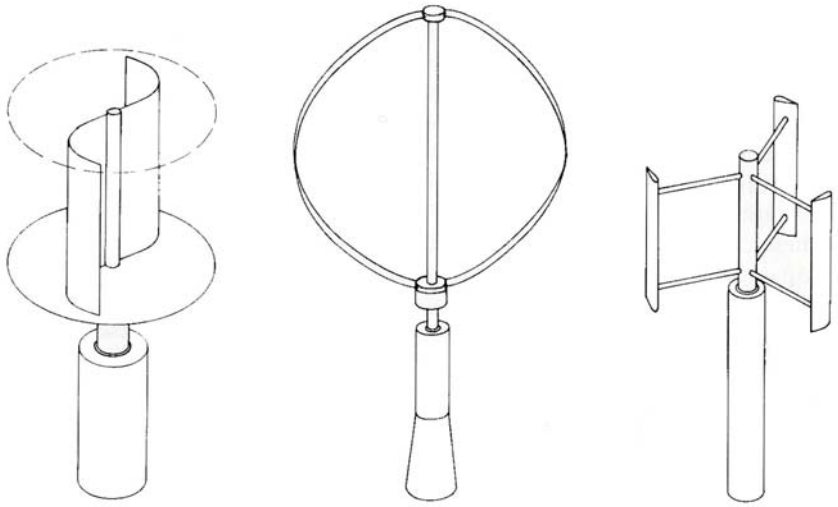

Figure 3.4. Savonius, Darrieus, and H-type rotor machines.
(Source: Hau 2000).

For the time being, vertical axis rotor concepts are generally not competitive with the horizontal axis wind turbines. Darrieus type rotor might have a potential for development with its advantage of ease design. First megawatt class Darrieus wind turbine is in Quebec with nearly 100m height, 64m diameter and 4.0 MW rated output.

3.2.2. Horizontal Axis Machines

Wind energy converters with their axis of rotation in a horizontal position are realized almost exclusively on the basis of propeller or turbine like concepts. This design, which comprises European windmills as much as the American wind turbine or modern wind turbines represents the dominating design principle of wind energy technology.

Rotor speed and power output can be controlled by pitching the rotor blades around their longitudinal axis. Blade pitching can be used as a highly effective protection against overspeed and extreme wind speeds, especially for large wind turbines. The rotor blade shape can be aerodynamically optimized and achieves its highest efficiency when the aerodynamic lift is exploited to maximum with lower drag force. These are the main advantages of this design. Figure 3.5 shows the schematic concept of a horizontal axis wind turbine. This type of turbines can be classified by two main concepts first of them is blade number and the other one is by determining the rotor position to wind as upwind or downwind. Nowadays largest capacity, in a horizontal axis wind turbine is three bladed upwind type, is 5 MW with a 126.3 m rotor diameter and 120m height tower installed in Hamburg/Germany.

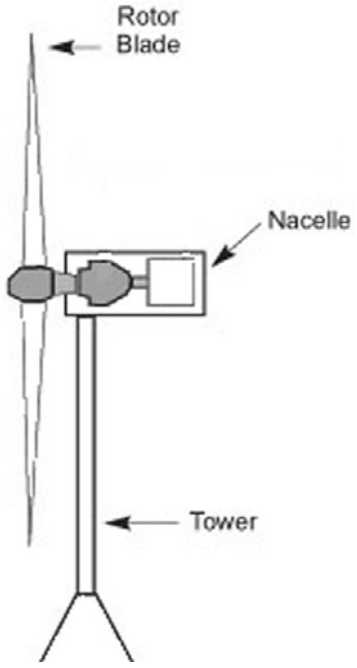

Figure 3.5. Scheme of a horizontal axis wind turbine.

Figure 3.6. Horizontal axis wind turbines installed in Alacati/Turkey.

3.3. Components of Horizontal Axis Wind Turbines

Main components of a wind turbine for electricity generation are the rotor, the transmission system, the generator, the yaw and control systems; their layout is shown in Figure 3.7. The major components are connected to nacelle, mounted on the tower, which can rotate according to the wind direction.

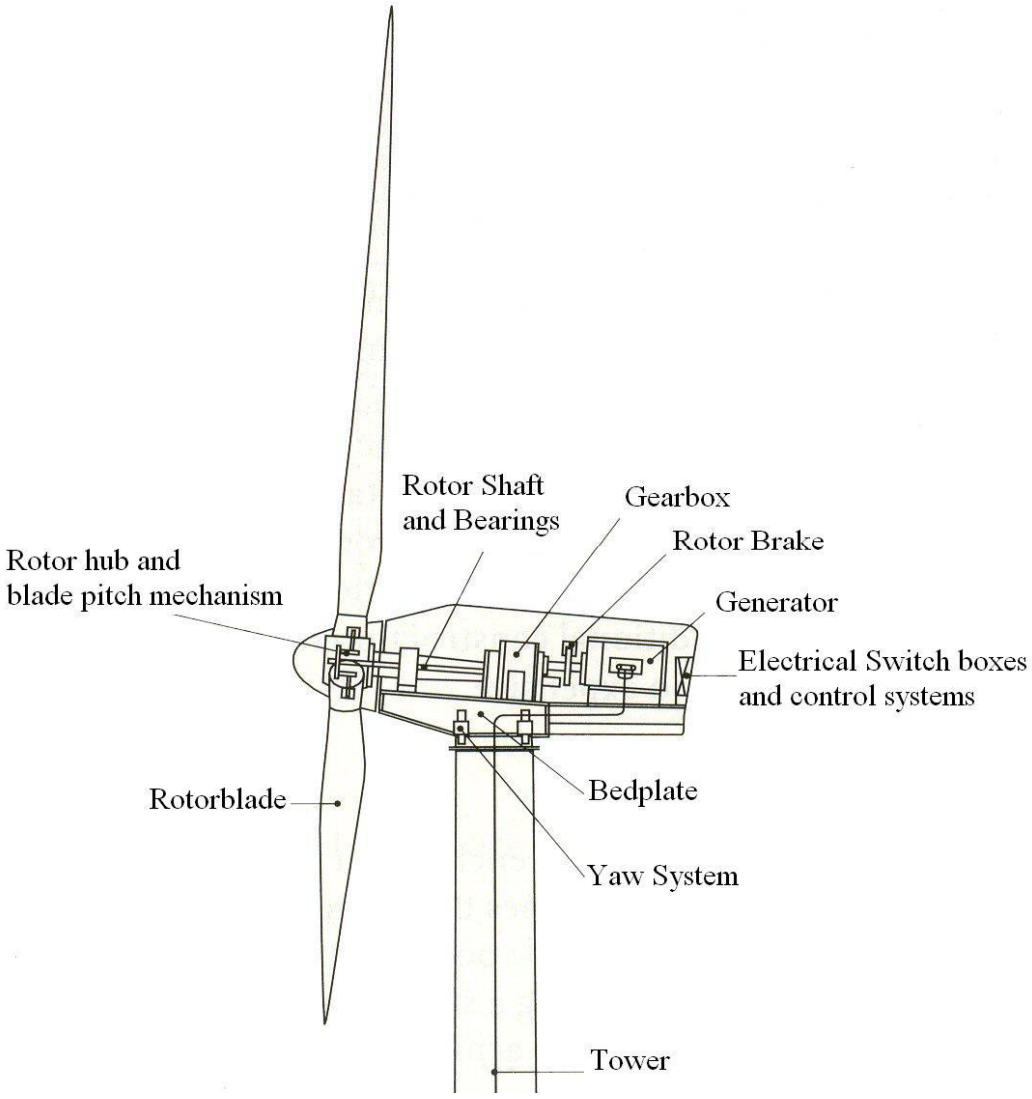

Figure 3.7. Main Components of a horizontal axis wind turbine.

3.3.1. Rotor Blades

The rotor is the first component of the functional units in a wind turbine. Therefore its aerodynamic and dynamic properties are essential factors for the whole system in many aspects.

The rotor's capability to convert the highest possible proportion of the wind energy flowing through the rotor swept area into mechanical power is obviously a result of its aerodynamic properties. The overall efficiency of energy conversion in the wind turbine is determined mainly by rotor.

The rotor blades of today's turbines reflect the different agreements between the optimum aerodynamic shape, the requirements of strength and stiffness and economical

manufacturing prospects. Blade material also plays a significant part in the design. Fiber-reinforced composites (glass fiber, carbon fiber and organic aramide fiber), steel, aluminum and wood/epoxy composite materials are suitable for blade production. Their aerodynamic properties will have investigated in Chapter 5.

3.3.2. Transmission System

The mechanical power generated by the rotor blades is transmitted to the generator by a transmission system located in the nacelle. This consists of a gearbox, sometimes a clutch, and a braking system to bring the rotor to rest in an emergency when not in operation. The gearbox is needed to increase the speed of the rotor, from typically 20 to 70 rpm to the 1000 or 1800 rpm which is required for driving most types of generator. The transmission system must be designed for high dynamic torque loads due to the fluctuating power output from the rotor.

3.3.3. Generator

All grid connected wind turbines drive three phase alternating current generators to convert mechanical energy to electrical energy. In very small wind turbines direct current generators are used for recharging batteries.

Generators producing direct current have the advantages of being operable at variable speed. They have a high maintenance requirement and are expensive. Three phase AC generators are used in conventional power plants.

Generators divided into two main classes. A synchronous generator operates at exactly the same frequency as the network to which its connected; synchronous generators are also called alternators. An asynchronous generator operates at a slightly higher frequency than the network; asynchronous generators are often called induction generators.

Induction generators and synchronous generators each have a non rotating part called the stator. The stators are similar for the two types of generator; they produce a rotating magnetic field at a constant speed. But their rotors are quite different. In a synchronous generator the rotor has a winding through which there passes a direct current; this is the field winding. The field winding creates a constant magnetic field

created by the stator winding. The rotor of an induction machine is quite different. It consists of a squirrel cage of bars, short circuited at each end. There is no electrical connection onto the rotor and the rotor currents are induced by the relative motion of the rotor against the rotating field of the stator.

The efficiency of synchronous machines is generally higher than in comparable induction machines like 1 to 2% in practice. Efficiency increases with increasing rated power (Hau 2000). Synchronous generators have the main advantage of controlling the direct current flowing. In a synchronous generator the direct current flowing in the field winding magnetizes the rotor, so by increasing the field current, reactive power may be exported to the grid. Similarly, by reducing the field current, reactive power may be drawn from the grid. Controlling the flow of reactive power gives control over the voltage of the power system. Synchronous generators impose less reactive power demand at the start (WEB_7 2005).

Here it may be needed to explain the relation between real, reactive and apparent power. Real power is the capacity to do useful work such as pump water or rotate a shaft against a load (kW). Reactive power is occurred by transformers or induction motors as magnetizing current for their iron cores but is generated by capacitors (kVAr). Finally apparent power is the vector addition of real and reactive power (kVA). The power factor is defined as the ratio of real power to apparent power.

Unlike a synchronous generator, which can operate at almost any power factor, the asynchronous generator draws reactive power depending on the real output. Without a real output the induction generator still gets a considerable reactive power to magnetize its iron core. Therefore capacitors are connected at the base of the wind turbine tower to provide reactive power or power factor correction (PFC). It is usual to provide PFC to compensate for the reactive power demand of the generator at zero output. Effect of PFC can be seen in Figure 3.8. At full output there is still some reactive power demand. It is possible to connect even more capacitors, but this can lead to hazardous over voltages in resonant condition, known as self-excitation, if the connection to the network is lost. Power correction factor is limited for the asynchronous generators in Turkey to 0.99 means reactive power is restricted with 1% of real power (TC Resmi Gazete 2004).

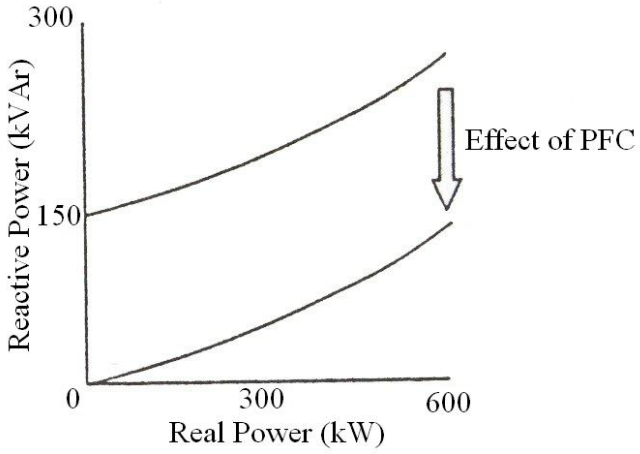

Figure 3.8. Operating characteristic of an asynchronous generator

The synchronous generator is more expensive for a given MVA size than the asynchronous machine and asynchronous generators can simply adaptable to variable speed generator systems.

3.3.4. Brake System

Very considerable forces are generated in high wind speeds. Effective brake systems are essential for the safe operation of wind turbines. Also arresting the rotor is necessary for servicing and repairs.

Brake system can be located on the slow or fast side of the gearbox. In most turbines; efforts to keep the brake disk diameter as small as possible lead to the installing the brake system on the fast shaft between gearbox and generator. However, installing the brake on the high speed shaft has at least two disadvantages. From the view of safety, the braking function fails if the low speed shaft or gearbox breaks down. They cause increased wear of the tooth flanks.

In some cases these disadvantages resulted in the installation of the brake system on the low speed rotor shaft. In small wind turbines a fully effective operating can be realized on the low speed side. In large wind turbine systems, for economical reasons this concept is therefore no longer common because of its considerable size.

3.3.5. Yaw System

A horizontal axis wind turbine has a yaw system that turns the nacelle according to the actual wind direction, using a rotary actuator engaging on a gear ring at the top of the tower. The wind direction must be perpendicular to the swept rotor area to avoid power loss. On the other hand, the yaw system may not react too sensitively, to avoid permanent small yaw movements which would reduce the life of the mechanical components.

A wind measurement system, usually mounted on the top of the nacelle, gets the wind speed and direction values. This measurement system provides a mean value of ten seconds. This value is compared with the instantaneous position, if the deviation is above approximately 5 degrees yaw system operates. In some design the nacelle is yawed to reduce power in high winds (Walker and Jenkins 1997).

Also the rotor can be oriented into the wind by wind vanes or fan-tail wheel. Nowadays, these methods no longer in use but some of the small scaled wind turbines operate with it.

3.3.6. Blade Pitch Mechanism

Most large wind turbines have rotors equipped with blade pitch control. The mechanism required to adjust the blade pitch angle for the rotor's power and speed control. A pitching range of around 20 to 25 degrees is enough for this purpose. But apart from this main function, a secondary task which has a considerable influence on the dimensioning of the blade pitch mechanism must be fulfilled. To brake the rotor aerodynamically, the rotor blades must be able to be pitched to the feathered position. This increases the pitch to approximately 90 degrees.

Blade pitch systems can be controlled by hydraulic drive or electrical drive systems. Hydraulic drives are still in majority in wind turbines. An alternative to hydraulic drive units are electrical motors. They can increasingly found in recent turbines. The reasons are the extended control possibilities of the newer electronically controlled pitching motors, and avoidance of leakage problems with hydraulic aggregates.

3.3.7. Tower

The tower is the main components of a horizontal axis turbine. This circumstance is both an advantage and a disadvantage. Disadvantageous are the costs involved, which can constitute up to 20% of the overall turbine costs. With the tower's increasing height, erection and servicing become increasingly difficult. On the other hand, the rotor's specific energy output also increases with tower height. Theoretically the optimal tower height occurs at the point where the two growth functions construction cost and energy yield intersect. In larger turbines, construction costs increase more rapidly with increasing tower height than in small turbines. Increase in the energy output with rotor hub height depends very much on the site's vertical shear wind exponent. Inland sites, above all, frequently have a considerably higher shear exponent than shore-based sites. Therefore economically valuable tower heights for inland siting are generally higher than those for shore-based applications. For example with large wind turbines with tower heights up to 80m and more an economic use of inland wind potential can be achieved.

Stiffness is the second important design parameter of a tower. Fixing the first bending natural frequency is a decisive factor for the design, the material required and construction costs. The goal of the tower design is to realize the desired tower height with the required stiffness at the lowest possible construction cost.

Steel or concrete materials are available for the construction. Steel designs range from lattice construction to tubular towers with or without guy cables. Concrete towers are the exception with series produced wind turbines.

CHAPTER 4

AERODYNAMICS OF ROTOR BLADES

The primary component of a wind turbine is an energy converter which transforms the kinetic energy contained in the moving air into mechanical energy. The extraction of mechanical energy from an air flow with the help of a wind energy converter follows its own basic rules.

Aerodynamics is the oldest science in wind energy. In 1922, Albert Betz was the first to predict the maximum power output of an ideal wind turbine, although Froude and Rankine had developed a similar approach for ship propellers before. Betz published between 1922 and 1925 that, by applying elementary physical laws, the mechanical energy extractable from an air stream passing through a given cross-sectional area is restricted to certain fixed proportion of the energy or power contained in the stream (Hau 2000). A major break-through was achieved by Glauert, by formulating the blade element momentum (BEM) method. This method extended with many 'engineering rules' is still the basis for all rotor design.

4.1. Actuator Disk Theory

In this model rotor becomes a homogenous disk that removes energy from the wind. The actuator disk provides a rational basis for illustrating that the flow velocity at the rotor is different from the free stream velocity. In this theory three assumptions are made; the flow is completely axial, the flow is rotationally symmetric and no friction occurs when the air passes the wind turbine rotor.

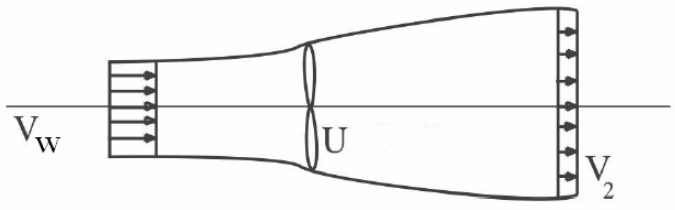

Figure 4.1. Axial Flow Model.

From the momentum theorem

$$T = \dot{m}_a (V_w - V_2) = \rho A U (V_w - V_2) \tag{4.1}$$

where T is thrust force on the disk (N), $\dot{m}_a$ is air mass flow rate through the disk (kg/s), V_w is free stream wind velocity, U is wind velocity at the disk (m/s), V_2 is wind velocity in the far wake (m/s) and A is disk swept area (m^2).

The power extracted from the actuator disk is

$$P_D = T \times U = \dot{m}(V_w - V_2) \times U \tag{4.2}$$

Energy loss per unit time from wind is:

$$P_w = \frac{1}{2}\dot{m}(V_w{}^2 - V_2{}^2) \tag{4.3}$$

From conservation of energy P_D=Pw. By combining Equations 4.2 and 4.3 we obtain wind velocity at the disk

$$U = \frac{V_w - V_2}{2} \tag{4.4}$$

Thus, the wind velocity at the disk is the average of the free stream and far wake velocities, so the total velocity change from free stream to far wake is twice the change from free stream to the disk. Let

$$V_w - U = aV_w \tag{4.5a}$$

Then

$$V_w - V_2 = 2aV_w \tag{4.5b}$$

$$a = \frac{V_w - U}{V_w} = \frac{V_w - \frac{V_w + V_2}{2}}{V_w} = \frac{V_w - V_2}{2V_w} \tag{4.5c}$$

$$U = (1 - a)V_w \tag{4.5d}$$

The term "*a*" is known as the axial induction factor and is a measure of the influence of the turbine on the wind. Because the minimum far wake velocity is zero, the maximum value of the induction factor is 0.5. The thrust is not of immediate importance, but the power is. From the first law of thermodynamics, assuming isothermal flow and ambient pressure in the far wake, power is equal to

$$P_D = \frac{1}{2}\rho AU\left(V_w{}^2 - V_2{}^2\right) = \frac{1}{2}\rho AU(V_w - V_2)(V_w + V_2) \tag{4.6}$$

where ρ is air density in kg/m^3. By combining Equations 4.5 and 4.6, the power from the actuator disk according to the Rankine-Froude theory, is

$$P_D = (4a(1-a)^2) \times (\frac{1}{2}\rho AV_w{}^3) = c_p \times P_{w0} \tag{4.7}$$

where c_p is power coefficient and P_{w0} is power in free stream (Mikkelsen 2003). From Equation 4.7, power coefficient gets its maximum value at *a*=1/3. Thus

$$C_{Pmax} = \frac{16}{27} = 0.593 \tag{4.8}$$

This is called "Betz Criterion" for maximum power extraction.

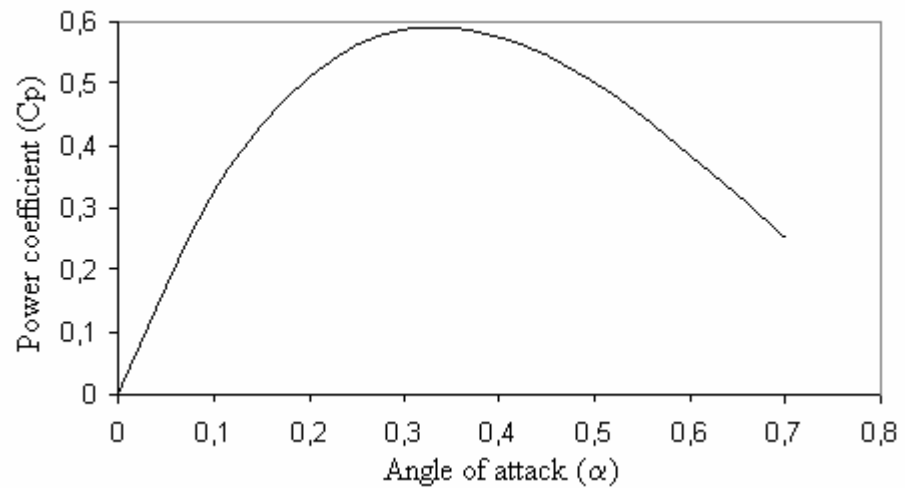

Figure 4.2. Graph shows Betz Criterion.

4.2. Blade Element Momentum Theory

Blade element momentum (BEM) theory is one of the oldest and most commonly used methods for calculating induced velocities on wind turbine blades. This theory is an extension of actuator disk theory, first proposed by the pioneering propeller work of Rankine and Froude in the late 19th century. The BEM theory, generally attributed to Betz and Glauert (1935), actually originates from two different theories: blade element theory and momentum theory. Blade element theory assumes that blades can be divided into small elements that act independently of surrounding elements and operate aerodynamically as two-dimensional airfoils whose aerodynamic forces can be calculated based on the local flow conditions. These elemental forces are summed along the span of the blade to calculate the total forces and moments exerted on the turbine. The other half of BEM, the momentum theory, assumes that the loss of pressure or momentum in the rotor plane is caused by the work done by the airflow passing through the rotor plane on the blade elements. Using the momentum theory, one can calculate the induced velocities from the momentum lost in the flow in the axial and tangential directions. These induced velocities affect the inflow in the rotor plane and therefore affect the forces calculated by blade element theory. This coupling of two theories ties together blade element momentum theory and sets up an iterative process to determine the aerodynamic forces and also the induced velocities near the rotor.

In practice, BEM theory is implemented by breaking the blades of a wind turbine into many elements along the span. As these elements rotate in the rotor plane, they trace out annular regions, shown in Figure 4.3, across which the momentum balance takes place. These annular regions are also where the induced velocities from the wake change the local flow velocity at the rotor plane. BEM can also be used to analyze stream tubes through the rotor disk, which can be smaller than the annular regions and provide more computational fidelity.

Because of its simplicity, BEM theory does have its limitations. One primary assumption is that the calculations are static; it is assumed that the airflow field around the airfoil is always in equilibrium and that the passing flow accelerates instantaneously to adjust to the changes in the vorticity in the wake. In practice, it has been shown that the airfoil response takes time to adjust to a changing wake resulting from new inflow or turbine operating conditions (Lissaman 1998). In order to model this time lag effect

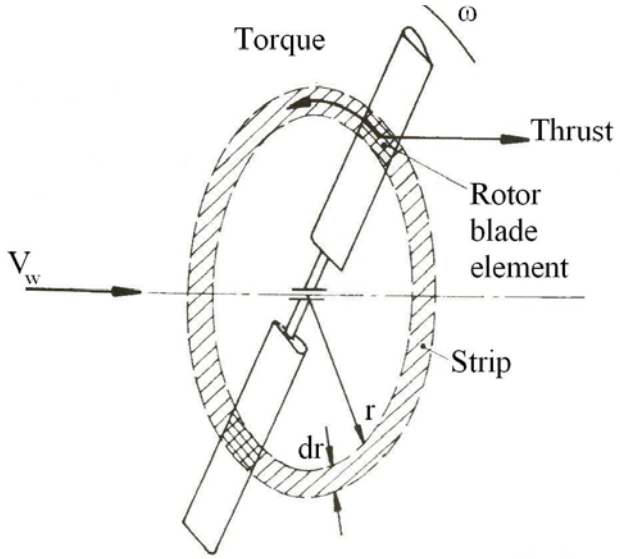

Figure 4.3. Annular ring generated by a blade element
(Source: Hau 2000).

correctly, the generalized dynamic wake model described below is used. One other limitation is that BEM theory breaks down when the blades experience large deflections out of the rotor plane.

Because the theory assumes that momentum is balanced in a plane parallel to the rotor, any deflections of the rotor will lead to errors in the aerodynamic modeling. Another limitation of BEM theory comes from blade element theory. This theory is based on the assumption that the forces acting on the blade element are essentially two-dimensional, meaning that spanwise flow is neglected. This assumption also implies that there is very little spanwise pressure variation, and the theory is therefore less accurate for heavily loaded rotors with large pressure gradients across the span. Some other limitations of the original theory include no modeling of tip or hub vortex influence on the induced velocities and an inability to account for skewed inflow. However, corrections to the original theory have provided some methods to model these aerodynamic effects and will be explained in more detail below. In spite of the limitations listed above, BEM theory has been used widely as a reliable model for calculating the induced velocity and elemental forces on wind turbine blades.

The advantage of the BEM theory is that each blade element is modeled as a two-dimensional airfoil. Figure 4.4 is an example of an airfoil with the velocities and angles that determine the forces on the element where, $a' = \frac{\omega}{\Omega}$, is angular induction factor, Ω, is turbine angular velocity, ω, is induced angular velocity, and, V_{total}, is local

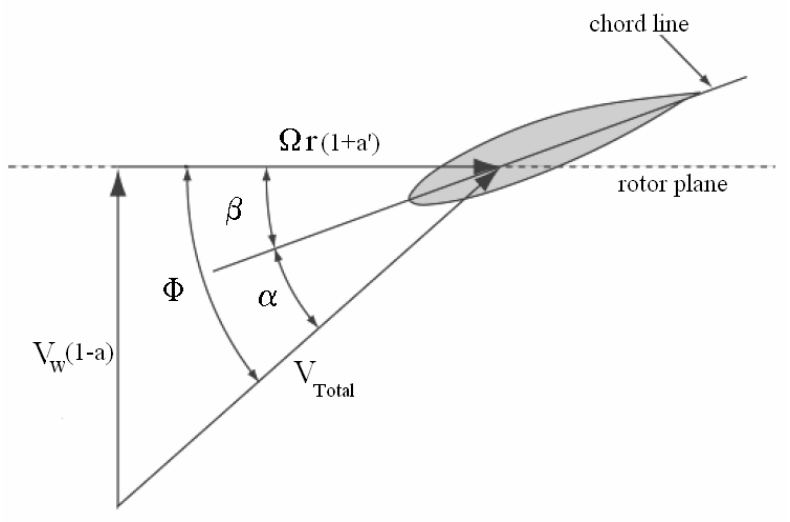

Figure 4.4. Velocities and angles acting on a blade at radius r.

velocity component. Figure 4.5 shows the resultant aerodynamic forces on the element and their components perpendicular and parallel to the rotor plane. These are the forces that dictate the thrust (perpendicular) and torque (parallel) of the rotor, which are the dominant forces for turbine design. In Figure 4.5, the angle relating the lift and drag of the airfoil element to the thrust and torque forces is the local inflow angle, Φ. As shown in Figure 4.4, this inflow angle is the sum of the local pitch angle of the blade, β, and the angle of attack, α. The local pitch angle is dependent on the static blade geometry, elastic deflections, and the active or passive blade pitch control system. The angle of attack is a function of the local velocity vector, which is in turn constrained by the incoming local wind speed, rotor speed and blade element velocities.

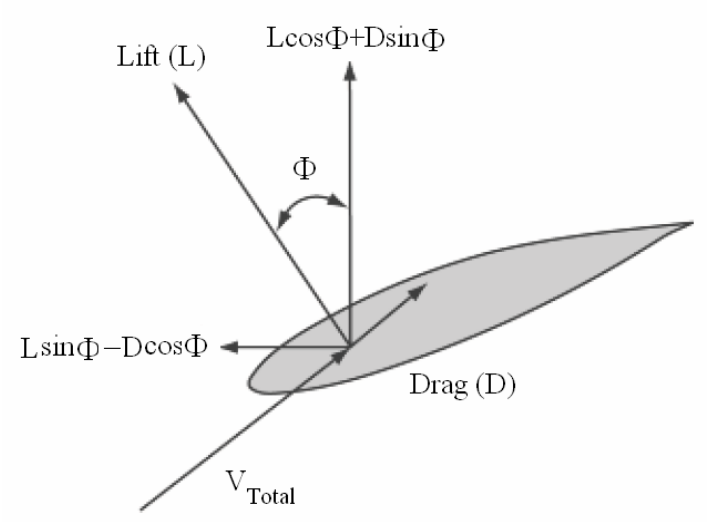

Figure 4.5. Local elemental forces.

The elemental lift and the elemental drag is expressed by blade element is:

$$\partial L = \frac{1}{2}\rho V_{Total}^2 C_L c dr \tag{4.9}$$

$$\partial D = \frac{1}{2}\rho V_{Total}^2 C_D c dr \tag{4.10}$$

where C_L and C_D are lift and drag coefficients and c is chord length in (m).

Because it is required to obtain the angle of attack to determine the aerodynamic forces on an element, firstly the inflow angle based on the two components of the local velocity vector must be determined. Assuming that the blade motion is very small, the resulting equation is dependent on the induced velocities in both the axial and tangential directions as well as the local tip speed ratio:

$$\tan\Phi = \frac{V_w(1-a)}{\Omega r(1+a')} = \frac{1-a}{(1+a')\lambda_r} \tag{4.11}$$

This equation holds for all elements of the blade along the span, although typically the inflow angle changes with element location. From blade element theory and Figure 4.5, the thrust distributed around an annulus of width *dr* (see Figure 4.3.) is equivalent to

$$\partial T = \partial L\cos\Phi + \partial D\sin\Phi \tag{4.12a}$$

If blade number is B

$$dT = B\frac{1}{2}\rho V_{Total}^2 (C_L\cos\Phi + C_D\sin\Phi)cdr \tag{4.12b}$$

and the torque produced by the blade elements in the annulus is equivalent to

$$dQ = B\frac{1}{2}\rho V_{Total}^2 (C_L\sin\Phi - C_D\cos\Phi)crdr \tag{4.13}$$

Now, to relate the induced velocities in the rotor plane to the elemental forces of Equations 4.12 and 4.13 incorporation of the momentum part of the theory, which states that the thrust extracted by each rotor annulus is equivalent to

$$dT = 4\pi r \rho V_w^2 (1-a) a dr \tag{4.14}$$

$$dQ = 4\pi r^3 \rho V_w \Omega (1-a) a' dr \tag{4.15}$$

is made (Wilson 1998). Thus, when two-dimensional airfoil tables of lift and drag coefficient as a function of the angle of attack, α, are included a set of equations that can be iteratively solved for the induced velocities and the forces on each blade element is obtained. However, before our system of equations is solved, several corrections to the BEM theory should be taken into account. These corrections include tip and hub-loss models to account for vortices shed at these locations, the Glauert correction to account for large induced velocities (a >0.4).

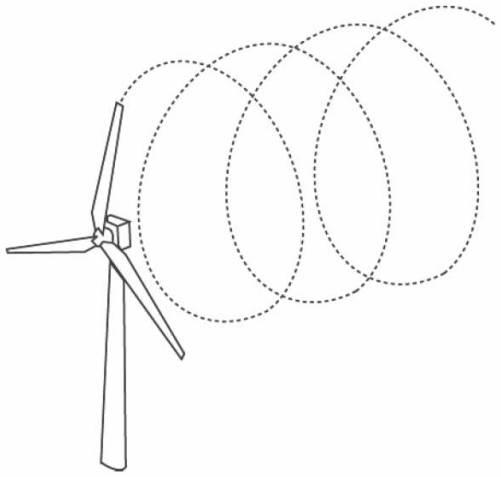

Figure 4.6. Helical wake pattern of single tip vortex.

4.2.1. Tip Loss Model

One of the major limitations of the original blade element momentum theory is that there is no influence of vortices shed from the blade tips into the wake on the induced velocity field. These tip vortices create multiple helical structures in the wake, as seen in Figure 4.6, and they play a major role in the induced velocity distribution at the rotor. The effect on induced velocity in the rotor plane is most pronounced near the

tips of the blades, an area that also has the greatest influence on the power produced by the turbine. To compensate for this deficiency in BEM theory, originally developed by Prandtl (Maalawi and Badawy 2001). Prandtl simplified the wake of the turbine by modeling the helical vortex wake pattern as vortex sheets that are convected by the mean flow and have no direct effect on the wake itself. This theory is summarized by a correction factor to the induced velocity field, F, and can be expressed simply by the following equation:

$$F = \frac{2}{\pi}\cos^{-1} e^{-f} \tag{4.16}$$

where

$$f = \frac{B}{2}\frac{R - r}{r \sin \Phi} \tag{4.17}$$

This correction factor is used to modify the momentum part of the blade element momentum equations, replacing Equations 4.14 and 4.15 with the following equations

$$dT = 4\pi r \rho V_W^2 (1 - a) a F dr \tag{4.18}$$

$$dQ = 4\pi r^3 \rho V_w \Omega (1 - a) a' F dr \tag{4.19}$$

When the tip-loss model is employed, the tip-loss factor sharply decreases as the radial position (r) along the blade (R) approaches the blade tip. This corresponds to a dramatic increase in the induction factor near the tip. As the induction factor increases, the resultant relative wind speed for a given blade segment decreases along with the angle of attack (Figure 4.7) . As a result, the loading (lift and drag forces) decreases near the tip.

4.2.2. Hub Loss Model

Much like the tip-loss model, the hub-loss model serves to correct the induced velocity resulting from a vortex being shed near the hub of the rotor. The hub-loss model uses nearly identical implementation of the Prandtl tip-loss model to describe the effect of this vortex, replacing Equation 4.17 with the following equation:

$$f = \frac{B}{2}\frac{r - R_{Hub}}{r\sin\Phi} \tag{4.20}$$

For a given element, the local aerodynamics may be affected by both the tip loss and hub loss, in which case the tip-loss and hub-loss correction factors are multiplied to create the total loss factor used in Equations 4.18 and 4.19.

$$F_{total} = F_{Hub} \times F_{Tip} \tag{4.21}$$

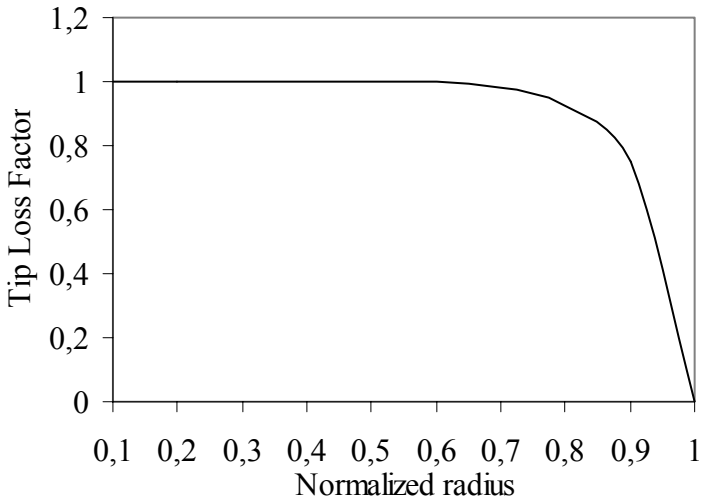

Figure 4.7. Tip loss factor for blade with constant inflow angle along span (for optimal twist angle).

4.2.3. Glauert Correction

Another limitation of the BEM theory is that when the induction factor is greater than about 0.4, the basic theory becomes invalid. This occurs with turbines operating at high tip speed ratios (e.g. constant speed turbine at low wind speeds), as the rotor enters what is known as the turbulent wake state ($a > 0.5$). According to momentum theory, this operating state results when some of the flow in the far wake starts to propagate upstream, which is a violation of the basic assumptions of BEM theory.

Physically, this flow reversal cannot occur, and what actually happens is more flow entrains from outside the wake and the turbulence increases. The flow behind the rotor slows down, but the thrust on the rotor disk continues to increase. To compensate for this effect, Glauert developed a correction to the rotor thrust coefficient based on experimental measurements of helicopter rotors with large induced velocities. While this model was originally developed as a correction to the thrust coefficient of an entire

rotor, it has also been used to correct the local coefficient of the individual blade elements when used with BEM theory. When the losses near the tip are high, the induced velocities are large; therefore, the possibility of a turbulent wake near the tips increases. Thus, for each element the total induced velocity calculation must use a combination of the tip-loss and Glauert corrections. Buhl derived a modification to the Glauert empirical relation that included the tip-loss correction as follows modification to the Glauert empirical relation that included the tip-loss correction as (Wilson 1998):

$$F_{Total} = \frac{8}{9} + (4F - \frac{40}{9})a + (\frac{50}{9} - 4F)a^2 \tag{4.22}$$

Solving for *a* we get,

$$a = \frac{18F - 20 - 3\sqrt{C_T(50 - 36F) + 12F(3F - 4)}}{36F - 50} \tag{4.23}$$

Figure 4.8 shows an example of the Glauert correction when the tip-loss factor is equal to one. When the induction factor, *a*, is 0.4 the BEM theory and Glauert correction produce the same value for thrust coefficient of 0.96. The slopes are also equivalent at this induction factor (Wilson 1998).

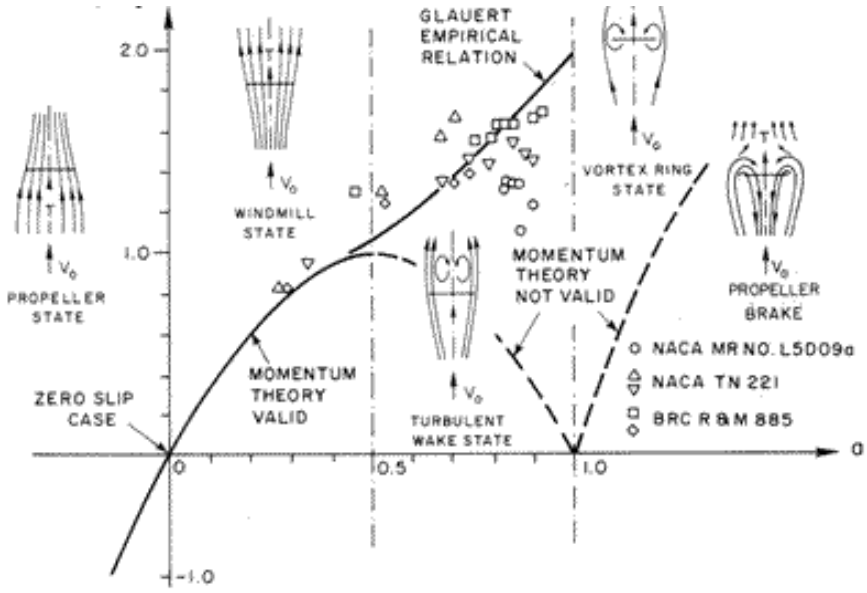

Figure 4.8. Relationship between the axial induction, flow state, and thrust of a rotor. (Source: Wilson 1998)

CHAPTER 5

ROTOR BLADE DESIGN

The rotor is the first component of the functional units in a wind turbine. Therefore its aerodynamic and dynamic properties are essential factors for the whole system in many aspects.

Rotor blade design relies heavily on aerodynamic theory. The blade is an aerodynamic body having a special geometry mainly characterized by an airfoil cross section. The optimization of a wind turbine's aerodynamic performance relies on many factors and variables for the selected airfoil sections, including blade number (B); blade pitch (β), the angle between the chord line and the plane of rotation; and tip speed ratio (λ), the ratio of peripheral tip speed to wind speed.

The rotor's capability to convert the highest possible proportion of the wind energy flowing through the rotor swept area into mechanical power is obviously a result of its aerodynamic properties. The overall efficiency of energy conversion in the wind turbine is determined mainly by rotor. Therefore the performance of the rotor can not be overrated in terms of economics.

5.1. Number of Rotor Blades

The number of blades is the first characteristic to determine. Solidity ratio is the ratio of blade area to swept area. The high number of blades means high solidity ratio, was used in old low tip speed ratio rotors for water pumping, the application which needs high starting torque but not high speed. Lower solidity ratios gives lower starting torque but operates at higher speed.

Because of the stability problems, number of blades must be odd. A rotor with an even number of blades will give stability problems for a machine with a stiff structure. The reason is that at the very moment when the uppermost blade bends backwards, because it gets the maximum power from the wind, the lowermost blade passes into the wind shade in front of the tower.

If the solidity of a wind turbine rotor is increased, the tip speed ratio for maximum power coefficient is reduced. This effect can be explained by considering a rotor of a given solidity at its peak power coefficient and associated tip speed ratio, producing its optimum axial induction. If the solidity of its rotor is increased and all other parameters are held constant, both lift and drag forces will increase and, as a result, the axial induction factor will increase beyond its optimum value. To restore optimum axial induction, aerodynamic forces on the blade must be decreased, which is accomplished by reducing the tip speed ratio.

In the blade element momentum theory each further rotor blade brings a little bit more power, but this is not running linear. The power increase from one to two blades is 10 % and the difference from two to three blades amounts to 3-4 percent only. The fourth blade only effects a power increase of 1 or 2 % (Hau 2000). In Figure 5.1 power coefficients versus tip speed ratios for different blades can be seen. The possible gain in power and energy yield of a few percent is not enough the cost of an additional rotor blade. So it is apparent why the modern wind turbines are two or three bladed.

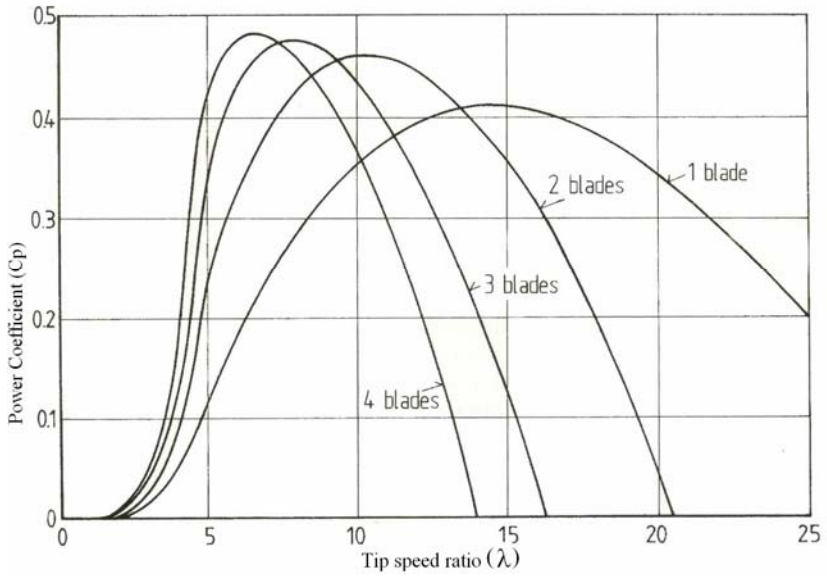

Figure 5.1. Power coefficients for different number of blades at different tip speed ratios.

(Source: Hau 2000)

Figure 5.2 shows the rotor power characteristics of various concepts. While windmills, which could essentially use only aerodynamic drag, achieved power coefficients of nearly 0.3 at the very most, modern wind rotors achieve power

coefficients of nearly 0.5. This also strongly emphasizes the importance of aerodynamic lift principle.

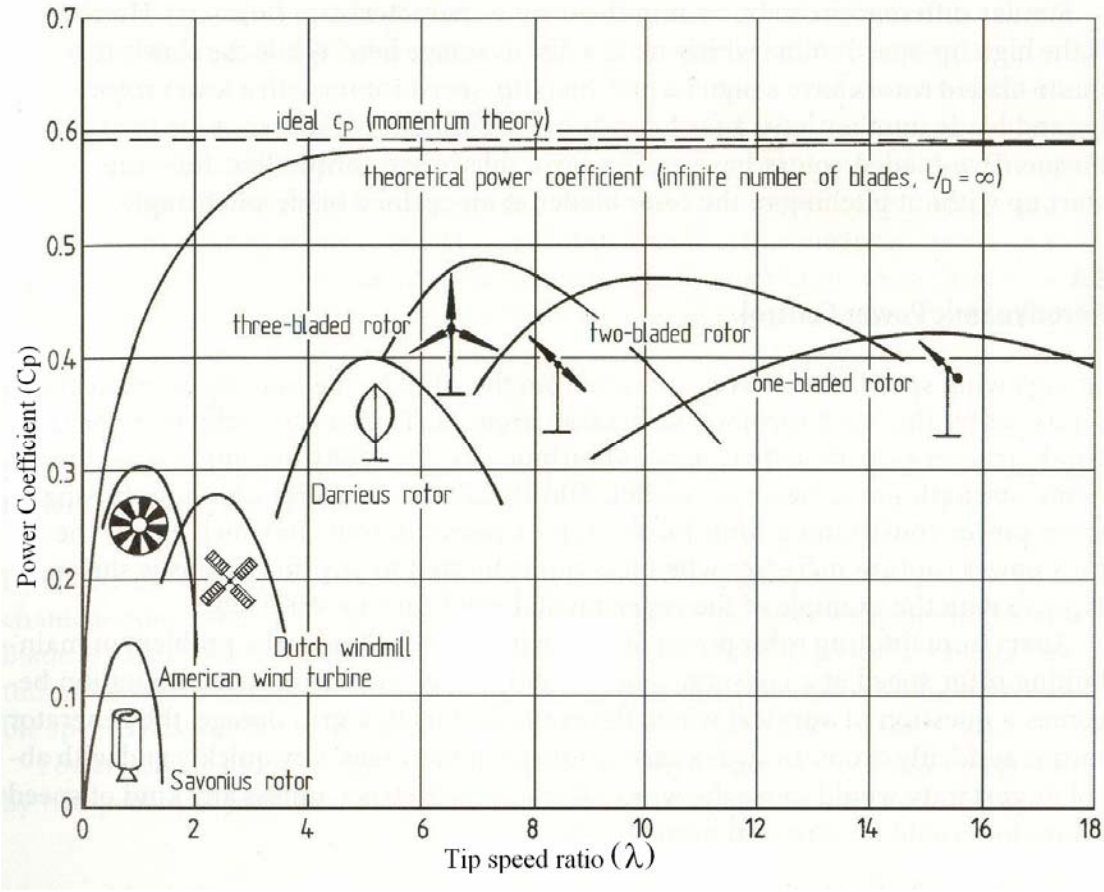

Figure 5.2. Power coefficients of various wind turbines.
(Source: Hau 2000)

5.2. Tip Speed Ratio

Tip speed ratio is the ratio of tangential speed of blade at tip to wind speed.

$$\lambda = \frac{\omega \cdot r}{V_w} \tag{5.1}$$

Its important design criteria to determine the optimum pitch angles along the blade. Also Modern generators work at higher rotational speeds thus higher tip speed ratios are used for design.

The profile of the c_p curves as a function of the tip speed ratio in Figure 5.2 also shows the optimal range of tip speed ratio for rotors varying numbers of blades. While

the three bladed rotor performs optimally at a design tip speed ratio of between 6 and 8, a two bladed rotor reaches its maximum c_p value at a tip speed ratio of nearly 10. The tip speed ratio of a one bladed rotor is about 15. The optimal tip speed ratio is a little bit dependent on the type of airfoil. However, only the maximum values of the c_p curves are significantly moves up or down by the airfoil characteristics. Therefore the correlation between blade number, power coefficient and optimal tip speed ratio are generally valid.

5.3. Rotor Blade Twist

The effective flow velocity increases from blade root to the tip because of the rotational speed. Also its angle of attack (α) also changes its values (see Figure 4.4). In order to obtain the optimal angle of attack the pitch angle (β) of the blades must decrease toward the tip. As a result rotor blades are twisted from root to tip. The twist angle is greatest at the root and the smallest at tip. In most of the designs twist angle is zero in 70-75% of rotor radius.

Determining the optimal blade twist can naturally only be done for a certain tip speed ratio. If design is done just for a rotor operating point, as a rule, this is the rated power operating point. The twist is not optimal for all other operating conditions, making efficiency losses unavoidable. Doing a design without any twist obviously leads to a considerable power loss.

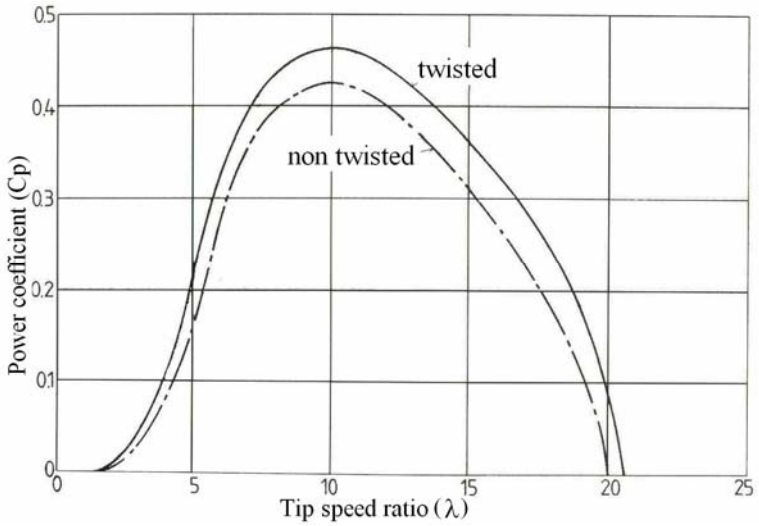

Figure 5.3. Power coefficients for twisted and non twisted blade design.

(Source: Hau 2000)

5.4. Airfoil

The efficiency of wind rotors with high tip speed ratio are to a great extent determined by the aerodynamic properties of the airfoils used. The influence of airfoil, characterized by the lift to drag ratio (L/D), on the rotor power coefficient can be represented in a general way. Airfoils are designed to generate lift force to create a force normal to the incident flow when immersed in this flow at a small angle to the airfoil's chord line. Lift forces operate through the generation of circulation and do not involve large viscous losses in the flow and the associated loss of total head, while drag forces function through flow separation on the blade and the loss of total head.

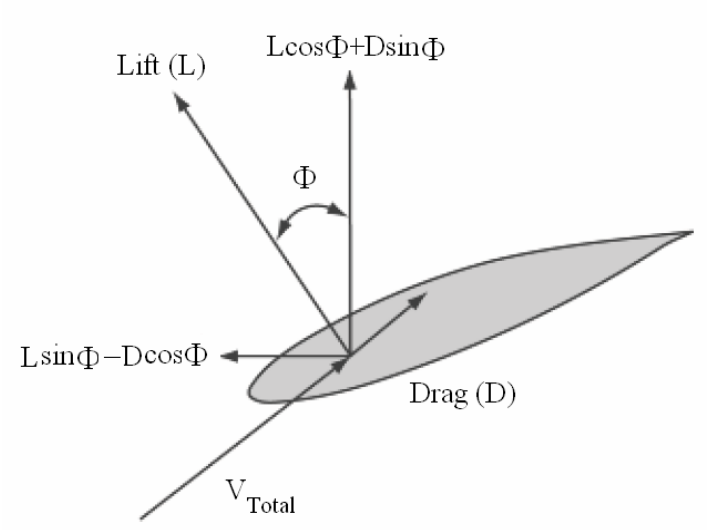

Figure 5.4. Local forces acting on airfoil.

When the lift to drag ratio drops the maximum power coefficient also decreases. The power coefficient's optimum shifts to lower design tip speed ratios. When lift drag ratio and tip speed ratio are high the number of rotor blades (B) has relatively little influence on the achievable power coefficient value, but when the L/D ratio and tip speed ratio are low, the number of blades has a higher significance. Therefore low tip speed rotors need more blades, but their airfoil characteristics are not so important. High tip speed rotors perform with fewer blades and the airfoil characteristics become an important factor for power generation.

The most significant flow factor influencing the behavior of low speed airfoils is that of viscosity, which indirectly causes lift and directly causes drag and flow

separation. This influence is characterized by the Reynolds number of the airfoil fluid combination. For an airfoil with a chord length of c (m) Reynolds number is:

$$\mathrm{Re} = \frac{V_{Total}.c}{\nu} \tag{5.2}$$

where V_{total} is relative velocity and ν is kinematic viscosity of air (m^2/s)

Generally, airfoil behavior is characterized by three flow regimes, as illustrated in Figure 5.5. The first of these is the attached regime, for angles of attack from about -15 to +15 degrees it varies with airfoil type; the second is the stall development regime, for angles of attack about between 15 and 30 degrees; thirdly, fully stalled or the flat plate state regime with attack angles between 30 and 90 degrees. These regimes are repeated in the other three quadrants, with approximate symmetry for drag and anti symmetry for lift (Lissaman 1998).

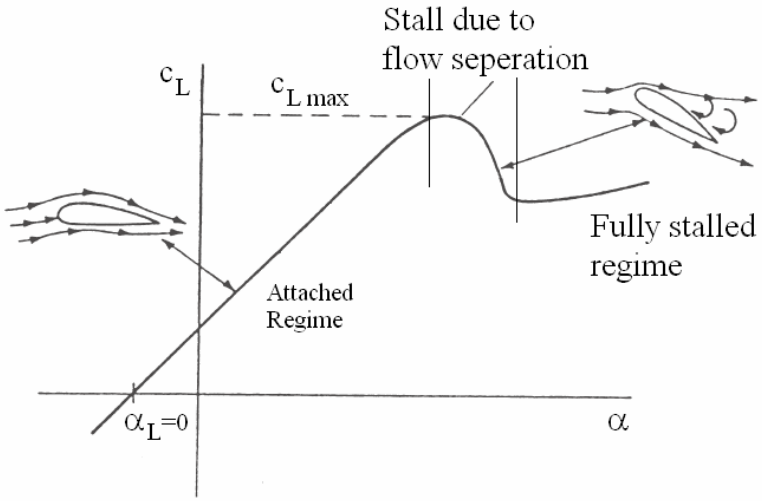

Figure 5.5. Typical airfoil aerodynamic characteristic C_L-α curve.

In the attached flow regime, the general airfoil behavior can be complicated and significantly affected by geometrical and viscous parameters like airfoil shape surface roughness and Reynolds number. The upper end of the attached flow regime is the region where separation and incipient stall generally occurs. Separation occurs because of the low pressure over the upper surface.

The next regime is stall development regime. Here the flow state ranges from initial incipient separation near the trailing edge of airfoil to massive separation over its

entire low pressure surface. Maximum lift coefficient occurs in this regime but also drag coefficient increases rapidly so designers must try to avoid work in post stall regime.

Airfoil behavior at angles of attack from approximately 30 to 90 degrees is similar to that of a similar flat plate. At 45 degree lift and drag coefficients are approximately equal and lift approaches zero near 90 degree. Like a flat plate, the drag coefficients in Figure 5.6 show a significant effect of *aspect ratio* (AR: span length divided by chord width), with the low aspect ratio case significantly lower in drag than the two dimensional situation.

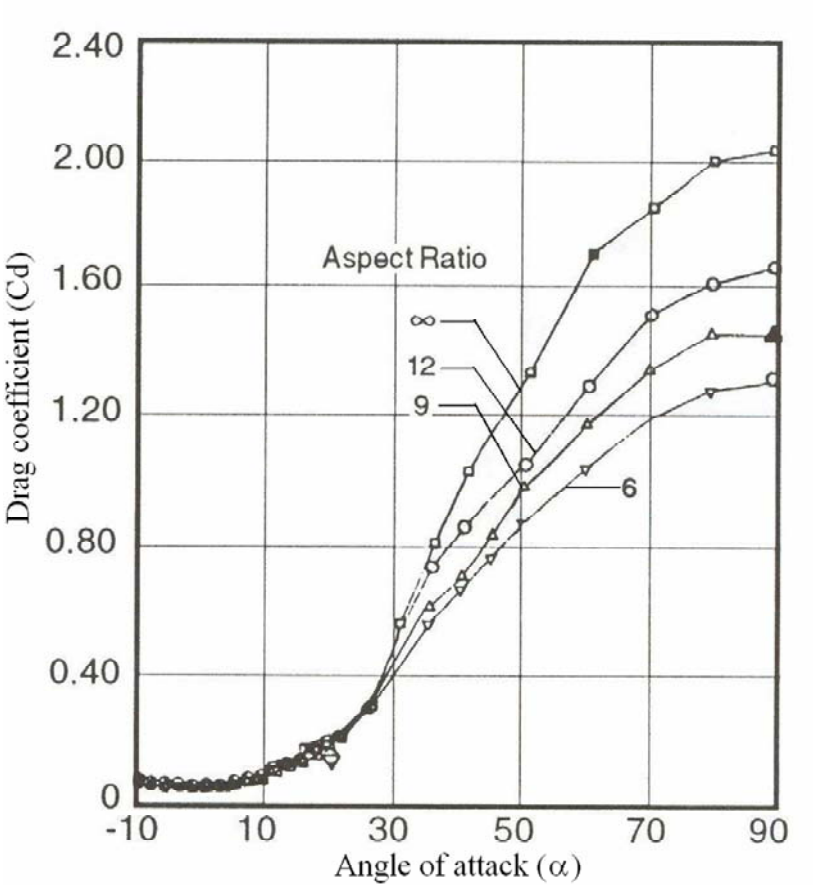

Figure 5.6. Drag coefficients with angle of attack and aspect ratio for an NACA 4415 airfoil at Re=0.5e06.

(Source: Lissaman 1998)

An empirical model for modifying two dimensional airfoil data in all three regimes to more accurately represent wind turbine rotor behavior has been developed by Viterna and Corrigan in 1981 (Tangler and Korucek 2005). Viterna equations require an initial angle of attack (α_{stall}) with its associated drag ($C_{D\ stall}$) and lift coefficient ($C_{L\ stall}$) along with a blade aspect ratio (AR). Results with Viterna equations are largely

dependent on the magnitude of the initial values of C_L and C_D. The blade AR selection is of lesser importance.

$$C_{D\max} = 1.11 + 0.018AR \tag{5.3}$$

$$C_D = B_1 \sin^2 \alpha + B_2 \cos \alpha \tag{5.4}$$

where,

$$B_1 = C_{D\max} \tag{5.5}$$

$$B_2 = \frac{C_{Dstall} - C_{D\max} \sin^2 \alpha_{stall}}{\cos \alpha_{stall}} \tag{5.6}$$

$$C_L = A_1 \sin 2\alpha + A_2 \frac{\cos^2 \alpha}{\sin \alpha} \tag{5.7}$$

where,

$$A_1 = \frac{B_1}{2} \tag{5.8}$$

$$A_2 = (C_{Lstall} - C_{D\max} \sin \alpha_{stall} \cos \alpha_{stall}) \frac{\sin \alpha_{stall}}{\cos^2 \alpha_{stall}} \tag{5.9}$$

Viterna equations are used, after stall development flow regime, to get post stall values of C_L and C_D at higher angles of attack.

Several airfoils can be select for the wind turbine blades. Larger lift drag ratios, stable C_{Lmax} values at stall and limited C_{Lmax} values at outboard region for control of peak power in high winds are typical design goals for selecting airfoil for horizontal axis wind turbines blade design.

Airfoils developed for airplane wings are also used in wind turbine rotors. This is justified as the flow speed in the aerodynamically important outer area of the rotor blades is comparable to the flight speeds of small commercial planes or propeller driven airliners. Nevertheless, the requirements made on airfoils for wind turbine rotors are not similar in every way to the requirements of aircraft design. For this reason special airfoils have been developed for wind turbines.

The most common aerodynamic airfoils in aviation have been compiled in airfoil catalogue by Doenhoff and Abbott (Abbott and von Doenhoff 1959). The first systematic airfoil developments for aircraft were carried out in 1923 to 1927 at an

aerodynamic research institute in Germany (Göttingen).Airfoils from the Göttingen airfoil system are hardly used today. They were practically replaced by the American NACA (National Advisory Committee for Aeronautics) airfoil series from 2 to 7. NACA 6 series are in use at wind blade design. NACA 6 series are designed for getting higher lift drag ratio and greater laminar flow region at higher speeds (Abbott and von Doenhoff 1959). But they experienced high C_D values outside of the design range.

Apart from NACA airfoils the laminar airfoils of the German Stuttgart Airfoil Catalogue developed by F.X. Wortmann are of importance (FX series). These airfoils were developed primarily for gliders, but they are also basically suitable for wind turbine rotors. Recently new airfoil series, designed exclusively for wind turbines, have been developed in the USA (the SERI and LS series), in the Aeronautical Institute of Sweden (FFA series), in the Delft University (DU series) and in the Riso National Laboratory at Denmark (Riso Series).

New generation airfoils aerodynamic measurements are compiled by Bertagnolio (Bertagnolio et. al. 2001). Some of the airfoils shapes is shown in Figure 5.7.

5.5. Chord Length

Beside the airfoil type chord length is another parameter effecting on Reynolds Number. A smaller chord reduces Reynolds number in accordance with equation 5.2.this is an aerodynamic reason avoiding large number of blades and narrow chord blades. The theoretical optimum chord length at any radial stations along the blade can be determined from the following equations (Manwell et al. 2002),

$$c = \frac{8\pi r \sin \Phi}{3BC_L \lambda_r} \tag{5.10}$$

where λ_r is local solidity ratio

$$\lambda_r = \frac{wr}{V_{total}} \tag{5.11}$$

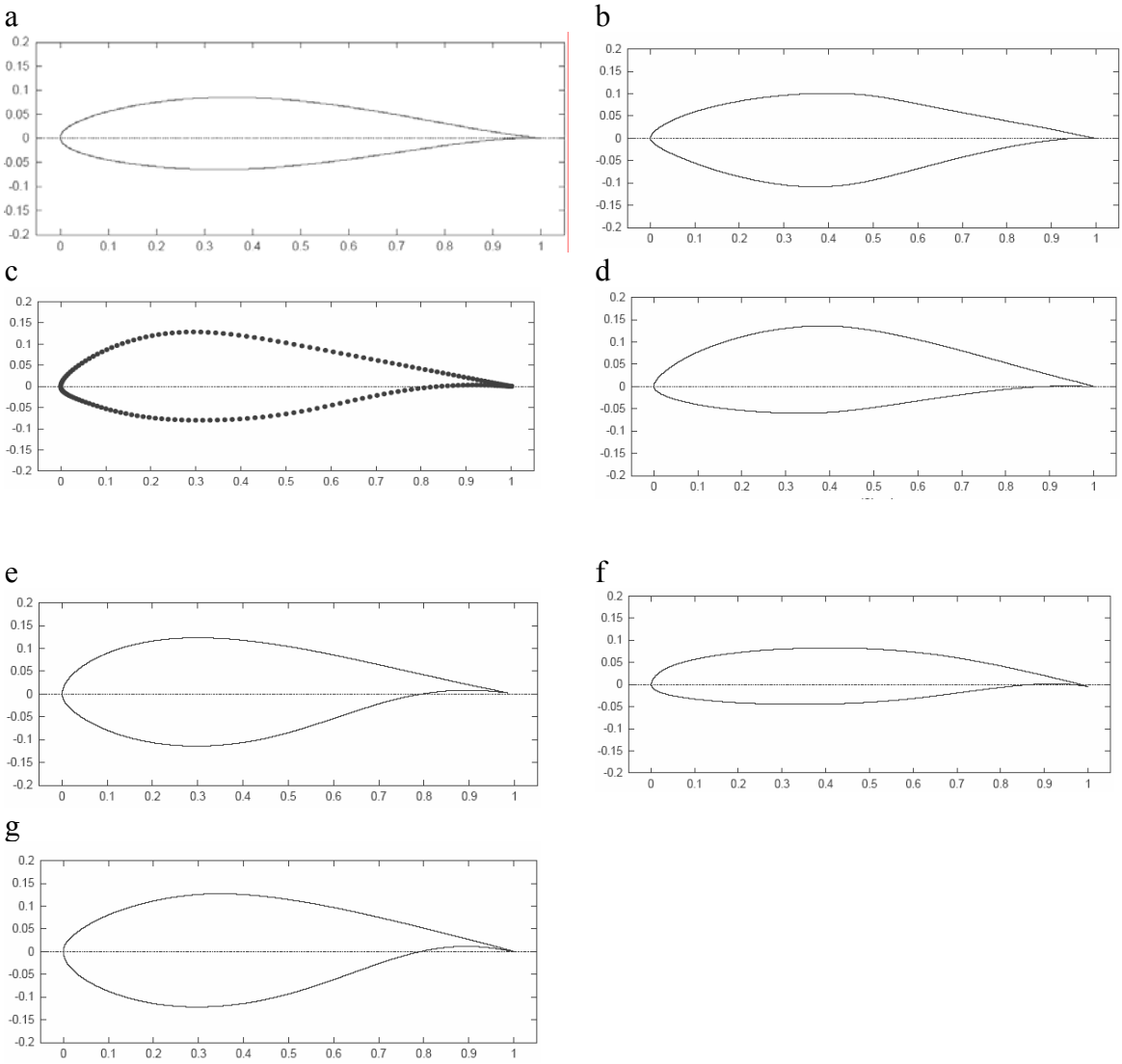

Figure 5.7. Common wind turbine airfoils. a.NACA 63215 b.S809 c.Riso A1/21 d.FX66-S196 e.FFA W3-241 f.LS-0413 g.DU 91-W2-250.
(Source: Bertagnalio et.al 2001)

5.6. Blade Length

Rotor's blade length can be determined from the rotor's area which depends in its value on the rated power of the wind turbine. The rated power can be calculated from rearranging the Equation 4.7 as

$$P_{rat} = \frac{1}{2}\rho V_{rat}^{3} A C_{p,rat} \qquad (5.12)$$

Where, A is the rotor swept area. For desired rated power we can calculate rotor blade length from the following equation:

$$R = \sqrt{\frac{P_{rat}}{\frac{1}{2}\rho V_{rat}^{3}\pi C_{p,rat}}} \tag{5.13}$$

CHAPTER 6

DEVELOPED MODEL

Design criteria of a wind turbine are described in the former chapters. In this chapter it will be proceeded to design a small scale wind turbine blade for the İzmir Institute of Technology campus area conditions.

6.1. Airfoil

It is known that rotor is the main essential factor for the whole system in the aerodynamic and dynamic meanings. Firstly it is needed to get aerodynamic properties of blade. For deciding to select the airfoil it is considered to make the blade work in attached flow regime with higher lift forces. Due to this, it is selected the airfoils used in horizontal axis wind turbines which are reported as working in higher angle of attacks without separation. FX66-S196, LS(1)413, S809 and Whisper H80's airfoils' aerodynamic properties are calculated for different angle of attacks with the help of a finite element solver program, FLUENT. Whisper H80's airfoil shape is nearly same as the NACA 63215 and it is assumed that the same airfoil shape is used for the entire blade.

6.1.1. Modeling Airfoil

In the present study the geometries are created and meshed using the preprocessor for geometry modeling and mesh generation which is called GAMBIT. The geometries are exported to the FLUENT program. Once a grid is transferred into FLUENT all remaining operations are performed within this software. These include setting boundary conditions, defining fluid properties, executing solution and post processing the results.

FLUENT is a computer program for modeling fluid flow and heat transfer in complex geometries. FLUENT provides complete mesh flexibility, solving flow problems with unstructured meshes that can be generated about complex geometries with relative ease. Supported mesh types include 2D triangular-quadrilateral, 3D

tetrahedral-hexahedral-pyramid-wedge, and mixed (hybrid) meshes. FLUENT also allows refining or coarsening grid, based on the flow solution. Airfoil aerodynamic properties are calculated in 2D solver.

In an external flow such as over an airfoil, it is needed to define a farfield boundary and mesh the region between the airfoil geometry and the farfield boundary. The farfield boundary is placed well away from the airfoil since the ambient conditions to define the boundary conditions will be used at the farfield. It is known that the farther from the airfoil, the less effect it has on the flow and so more accurate is the farfield boundary condition. Farfield which is used can be seen in Figure 6.1, where "c" is chord length.

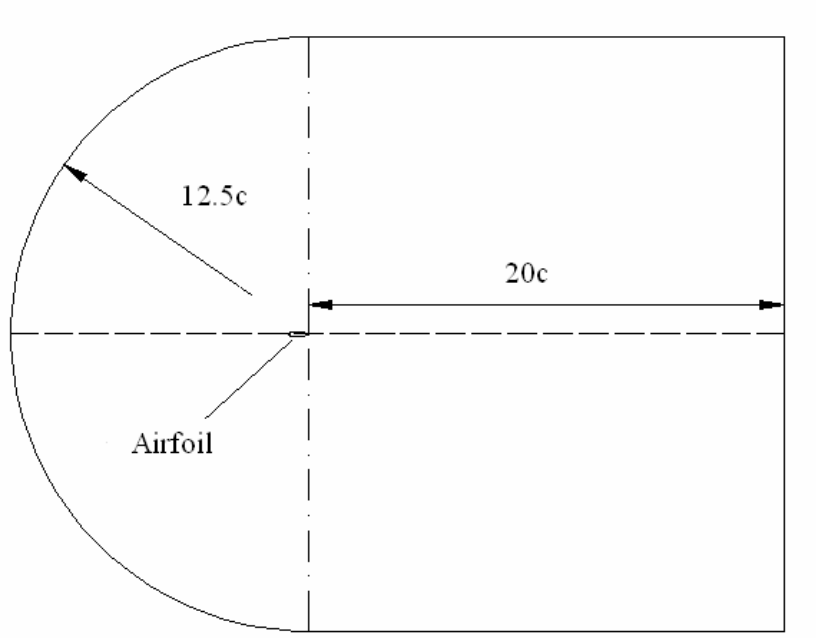

Figure 6.1. Farfield boundary distances.

In meshing the model the most resolution is needed close to the surface near the leading and trailing edges since these are critical areas with the steepest gradients. Cluster points are made near the airfoil since this is where the flow is modified the most; the mesh resolution as we approach the farfield boundaries is progressively coarser since the flow gradients approach zero. 2D Quadrilateral mapped mesh method used for these conditions. Biggest size of mesh used on airfoil surface size is 0.02. Model grid distributions for all faces and close to the airfoil are given in Figures 6.2, 6.3 and 6.4.

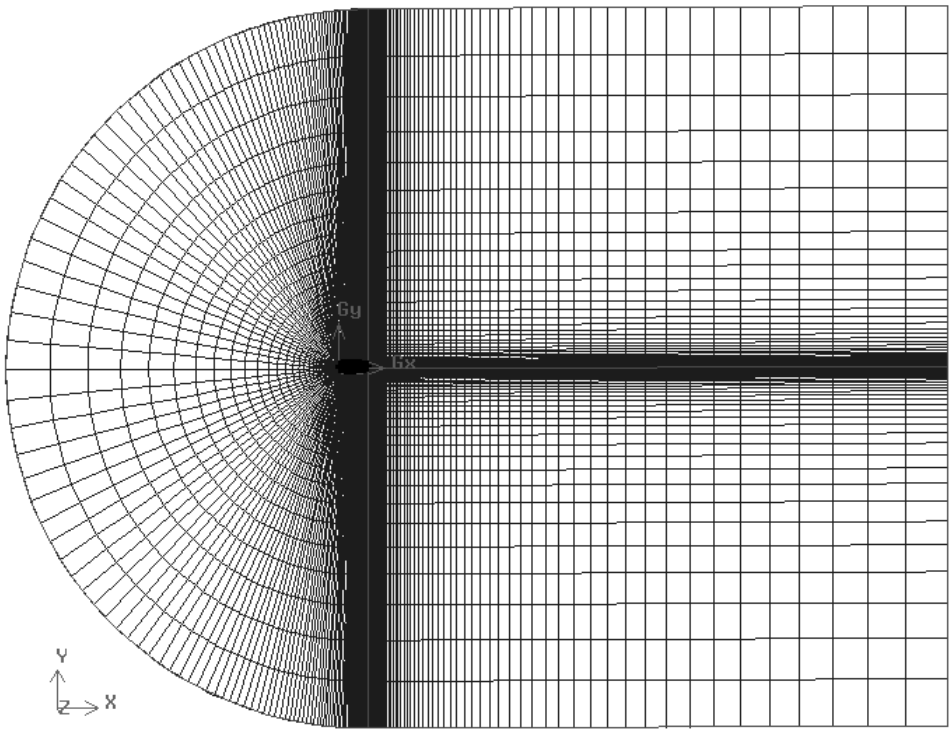

Figure 6.2. Grid distribution over the system.

Created meshes are exported to the FLUENT program where problem definition is completed by specifying physical models and boundary conditions for the models

Segregated implicit solution algorithm is used. Using segregated approach, the governing equations are solved sequentially (i.e., segregated from one another). Because the governing equations are non linear, several iterations of the solution loop must be performed before a converged solution is obtained. Each iteration consists of the steps illustrated in Figure 6.5. In the segregated solution method non-linear governing equations are linearized to produce a system of equations for the dependent variables in every computational cell. Implicit means, for a given variable, the unknown value in each cell is computed using a relation that includes both existing and unknown values from neighboring cells. Therefore each unknown will appear in more than one equation in the system, and these equations must be solved simultaneously to give the unknown quantities.

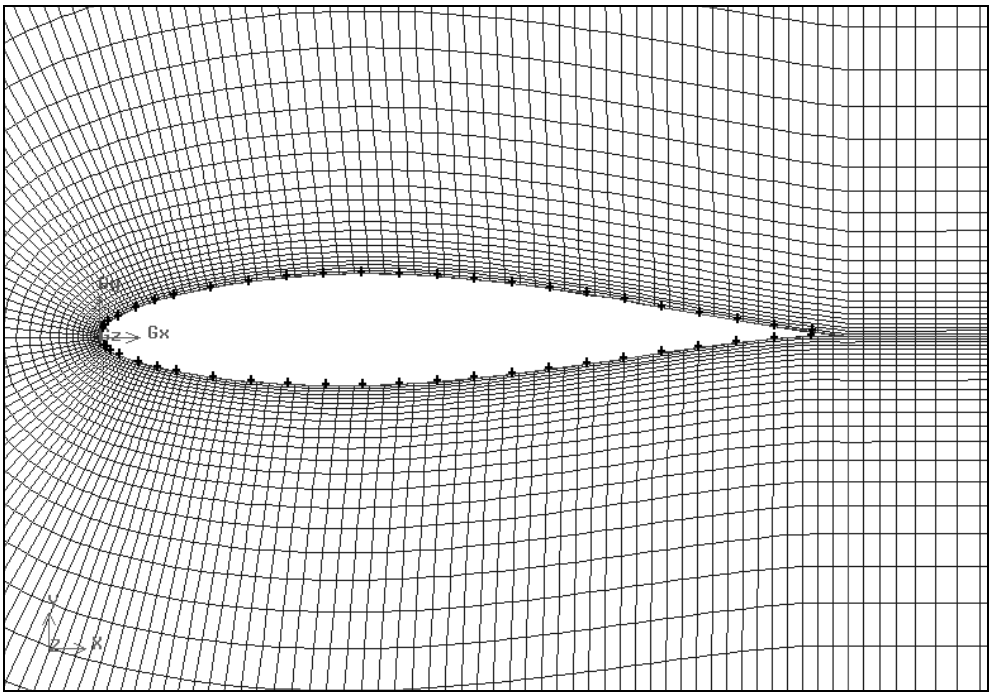

Figure 6.3. Grid distribution close to the airfoil.

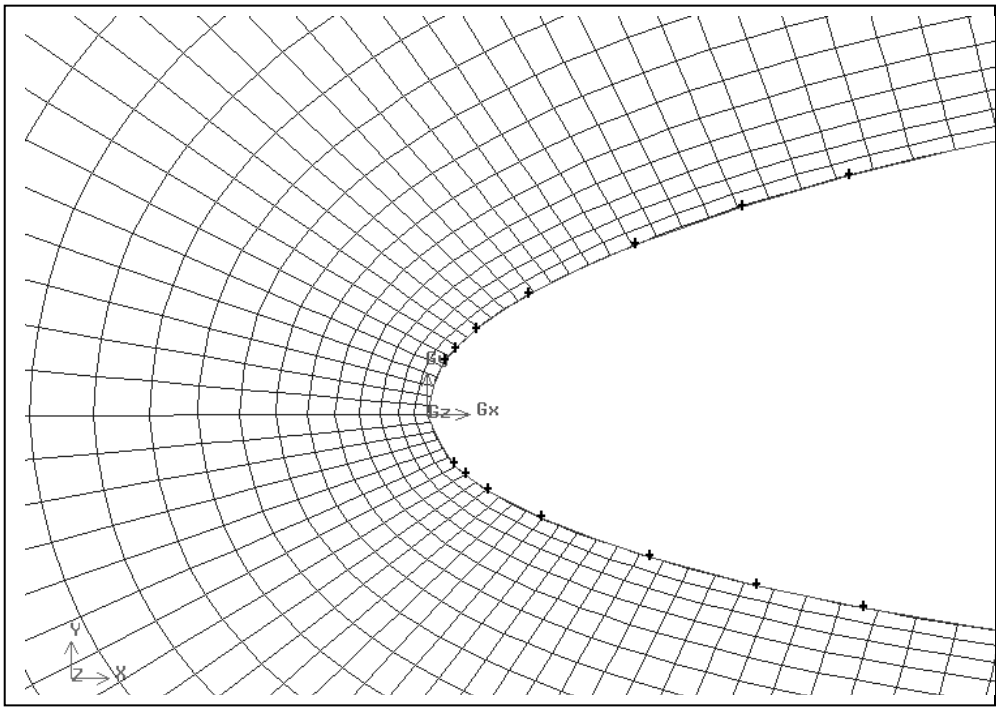

Figure 6.4. Grid distribution close to the leading edge of airfoil.

.

The Spalart-Allmaras turbulence model is used for the specification of the flow, which is designed specifically for aerospace applications involving wall bounded flows (Fluent 1999). The model can be considered a more practical alternative to large eddy simulation (LES) for predicting the flow around high-lift airfoils (Fluent 2003).

Air with a constant density of 1.225 kg/m^3 is taken as fluid material. For comparing the results with the experimental ones, same Reynolds number is taken. Operating pressure is taken as 101325 Pascal. Farfield in the backside of the airfoil is set as pressure outlet with a gauge pressure of 0 and the other farfields are set as velocity inlet.

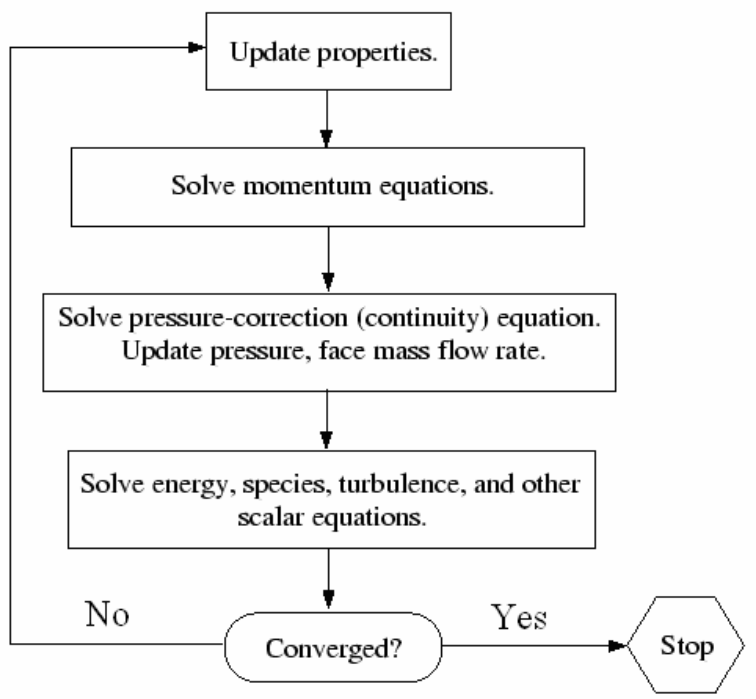

Figure 6.5. Overview of the segregated solution method.

After specifying the physical models and boundary conditions, the calculation starts from arbitrary initial conditions (except at the boundaries) and converges to the correct solution after performing a number of iterations. For different attack angles different velocity components are set as velocity inlets and, lift and drag forces are monitored.

$$V_x = V\cos\alpha \tag{6.1a}$$

$$V_y = V\sin\alpha \tag{6.1b}$$

We selected LS(1)413 for root section and FX66-S196 for tip section. LS(1)413 is selected for higher lift forces for root to obtain early wake. But at the tip more stable airfoil is needed, for this reason FX66-S196 is selected for tip section to get control of peak power. Also FX66-S196 has a stable lift coefficient, at high angles of attack, relatively from other airfoils.

6.2. Blade Length

Blade length is calculated from rated power with equation 5.13. Rated Power of Whisper H80 is reported as 1000 W at 12.5 m/s wind speed. For comparison we will use the same blade length is used the proposed for design. Blade length is 115 cm with extensions and hub diameter its rotor radius is 3 meters. Rated power for mean wind speed of 6.85 m/s at hub height of 10 m at Iztech campus is 484.9 watts for this rotor diameter.

6.3. Tip Speed Ratio and Pitch Angle

Tip speed ratio is calculated as 5.89 for angular velocity of 275 rpm. For this tip speed ratio inflow angle is calculated from corrected Glauert Equations (Maalawi and Badawy 2001).

$$\tan\phi = \frac{1-\mathrm{a}}{\lambda_{\mathrm{r}}\left(1+\mathrm{a}'\right)} \tag{6.2}$$

$$\mathrm{a}' = \frac{1-3\mathrm{a}}{4\mathrm{a}-1} \tag{6.3}$$

$$\mathrm{a} = \frac{1}{2}\left[1-\Lambda_{\mathrm{r}}\left(\cos\theta^{+}-\cos\theta^{-}\right)\right] \tag{6.4}$$

$$\theta^{\pm} = \frac{1}{3}\cos^{-1}\left(\pm\Lambda_{\mathrm{r}}^{-1}\right) \tag{6.5}$$

$$\Lambda_{\mathrm{r}} = \sqrt{1+\lambda_{\mathrm{r}}^{2}} \tag{6.6}$$

6.4. Chord Length

Chord lengths are calculated from Equation 5.10 and smooth transition is obtained between 0.7 and 0.8 m where the used airfoil is changed.

6.5. Blade Performance Calculations

Before calculating performance of rotors, calculations are done for extrapolated airfoil tables for higher angle of attacks with Viterna method. Results given in Appendix A are transferred and problem solved with a blade element momentum theory using software (WTPERF) written by Buhl which is also used by National Renewable energy Laboratories of US (NREL).

CHAPTER 7

RESULTS

In this chapter, results of aerodynamic calculations of various airfoils, design parameters of new designed blade and performance calculations of new designed rotor will be introduced.

7.1. Airfoil Characteristics

Experimental measurements of LS (1) 413, NACA 63215 were taken from the book of Abbott and von Doenhoff (Abbott and von Doenhoff 1959). Measurements for NACA 63215 for Reynolds number of 1.1e06 was taken from Fuglsang which was done at Velux Wind Tunnel (Fuglsang et. al. 1998). FX66-S196 measurements were done in the Laminar Wind Tunnel at the Institute for Aerodynamics and Gasdynamics of Stuttgart (Riso 2001). S809 values were measured in the low-turbulence wind tunnel at Delft University of Technology by Somers (Somers, 1997). For S809 calculations of Riso Institute was taken into comparison because of lack of the experimental values for higher angle of attacks.

Results are shown in Figures 7.1-4. It's seen that there is a good agreement between experimental data and calculated values. Lift curves are similar with a little shifted experimental values. It is also observed that results fit better with newer experimental results as in NACA63215 calculations and Velux measurements. So it can not be assessed that numerical code is responsible for discrepancies. For determining the behavior of airfoils at lower Reynolds numbers and make comparable calculations, are done with V=8 m/s wind speed (Re=5.5e05). Comparison of lift coefficients and drag coefficients for different angles of attack are shown in Figures 7.5 and 7.6.

Velocity magnitudes and vectors at stall development regime and post stall (fully stalled) regime for airfoil shapes are shown in Figures 7.7-22. Different separation points are observed for different airfoils.

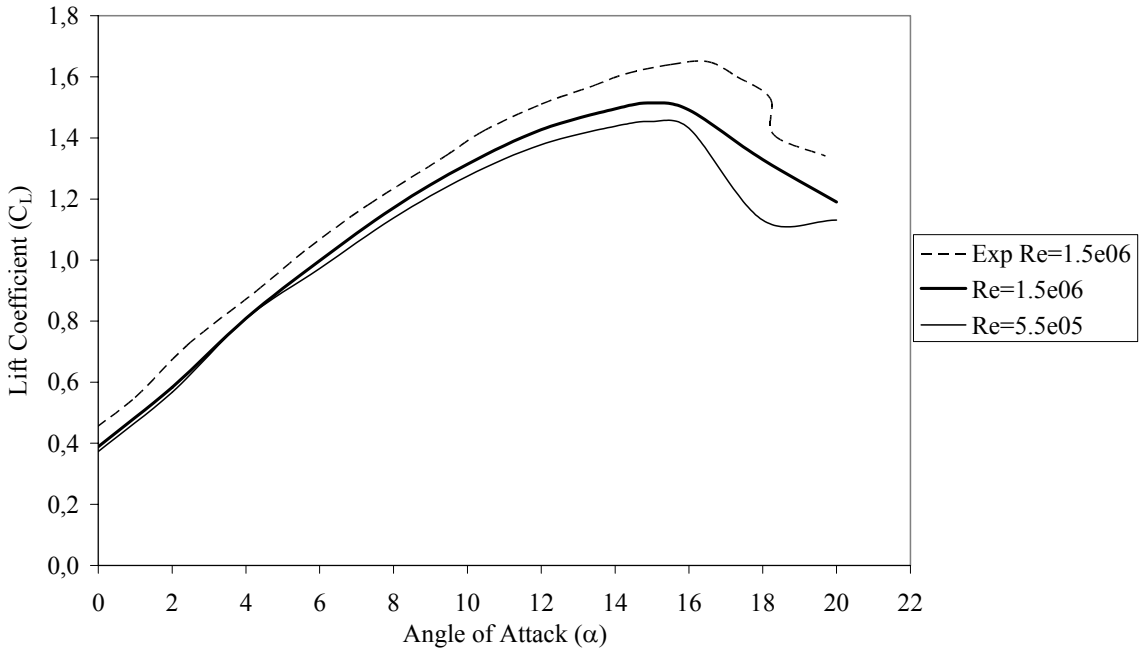

Figure 7.1. Lift coefficients versus angle of attack for LS (1) 413.

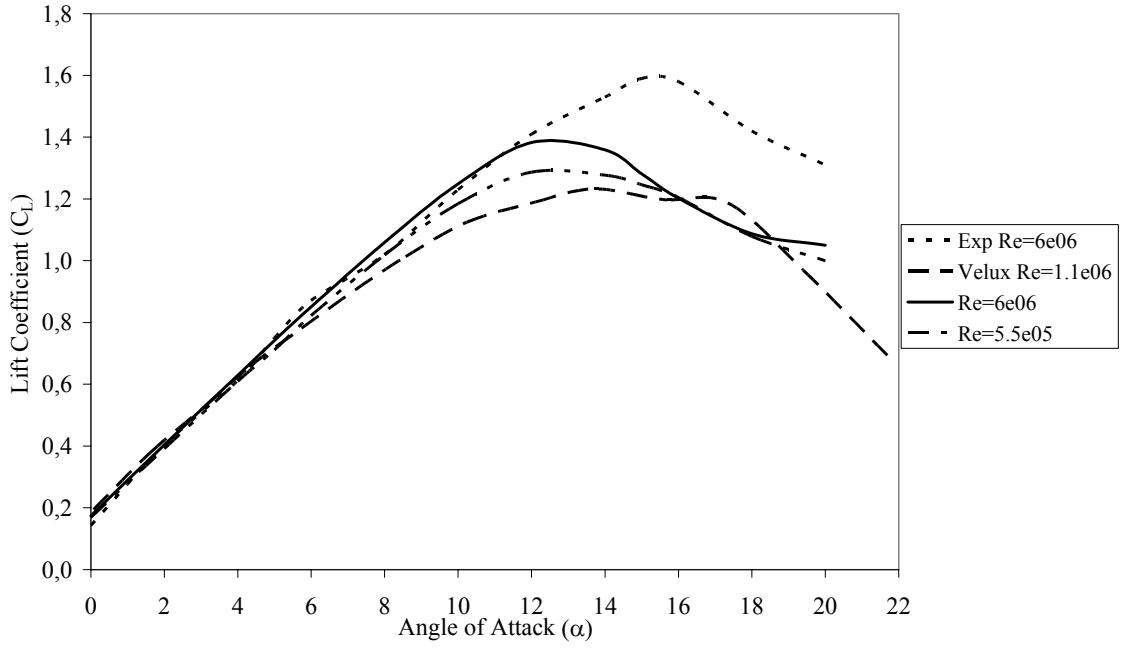

Figure 7.2. Lift coefficients versus angle of attack for NACA 63215.

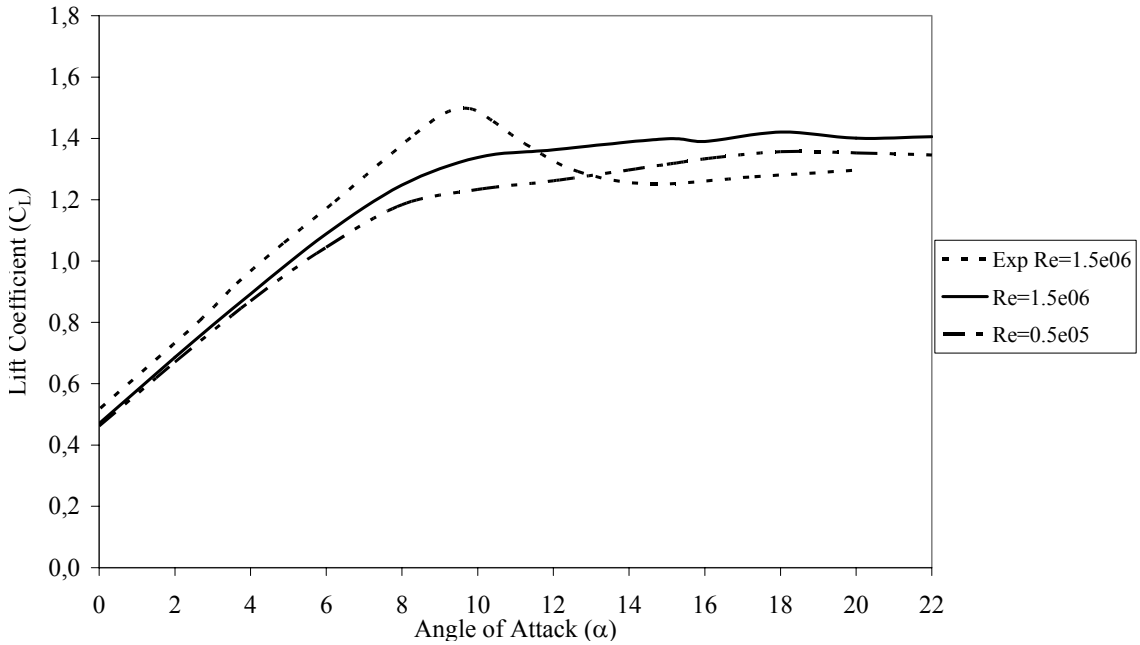

Figure 7.3. Lift coefficients versus angle of attack for FX66-S196.

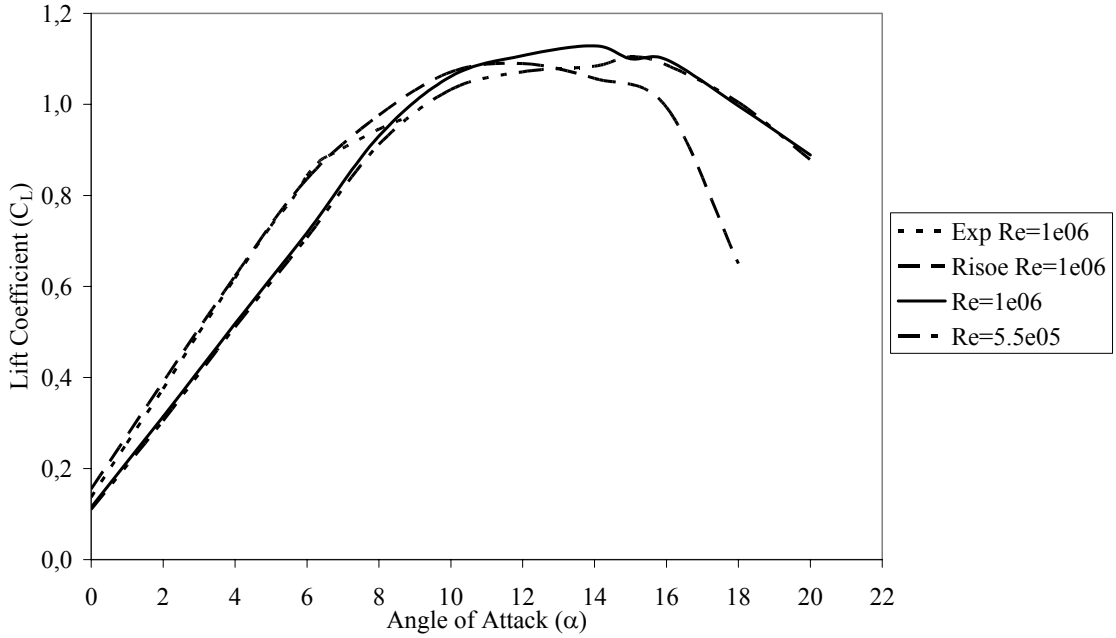

Figure 7.4. Lift coefficients versus angle of attack for S809.

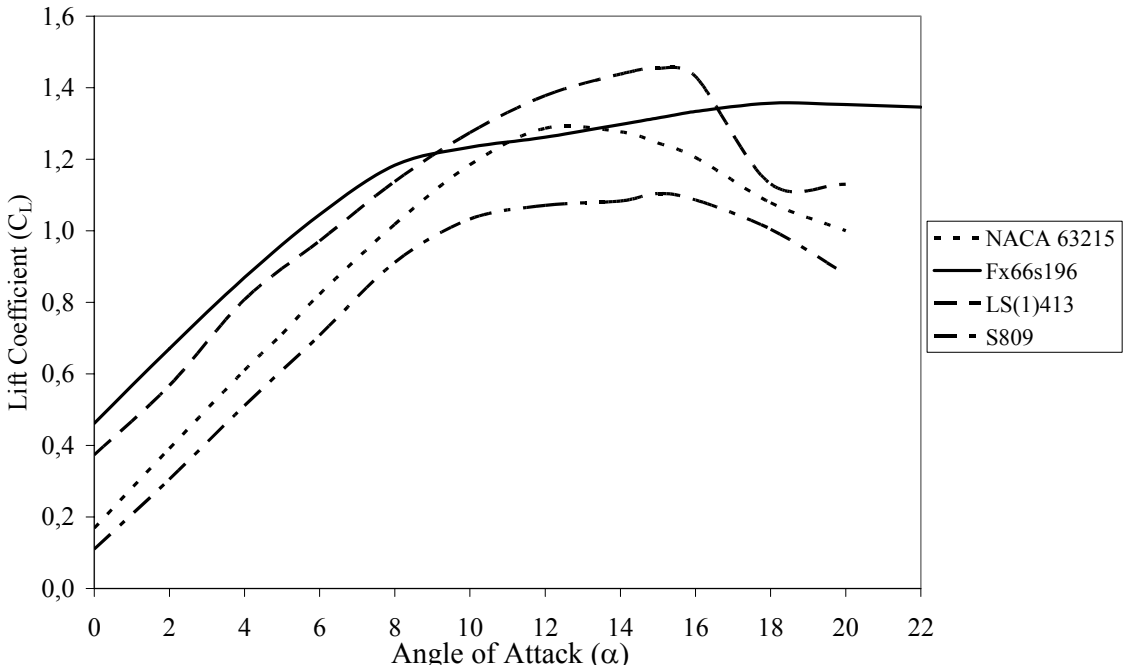

Figure 7.5. Lift coefficients versus angle of attack for Re=5.5e05.

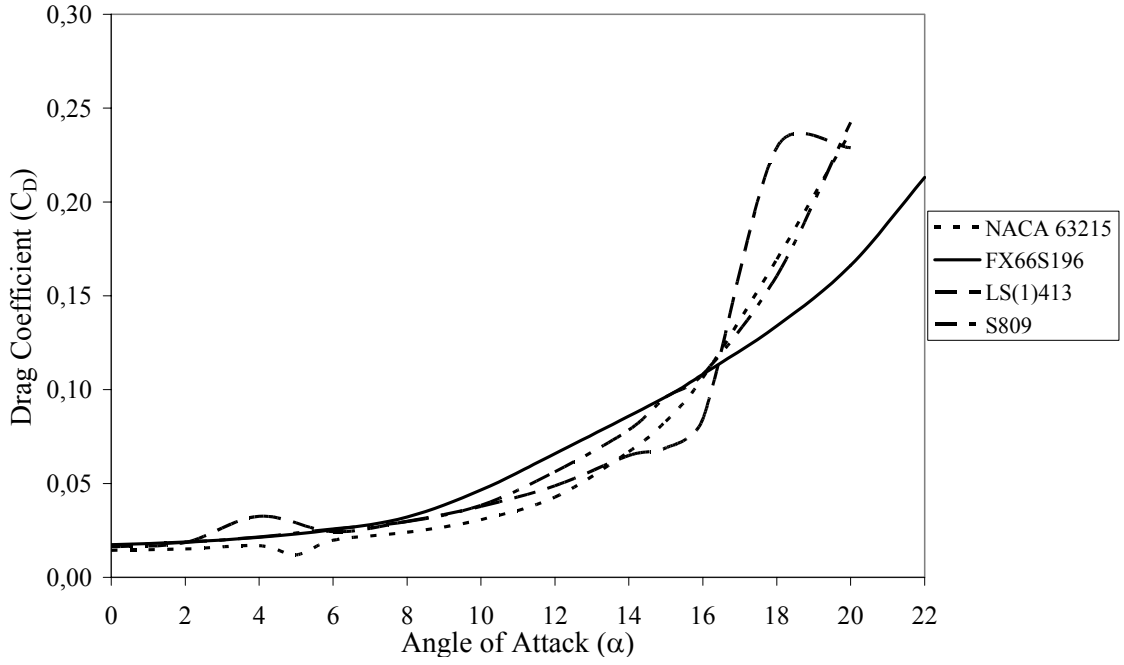

Figure 7.6. Drag coefficients versus angle of attack for Re=5.5e05.

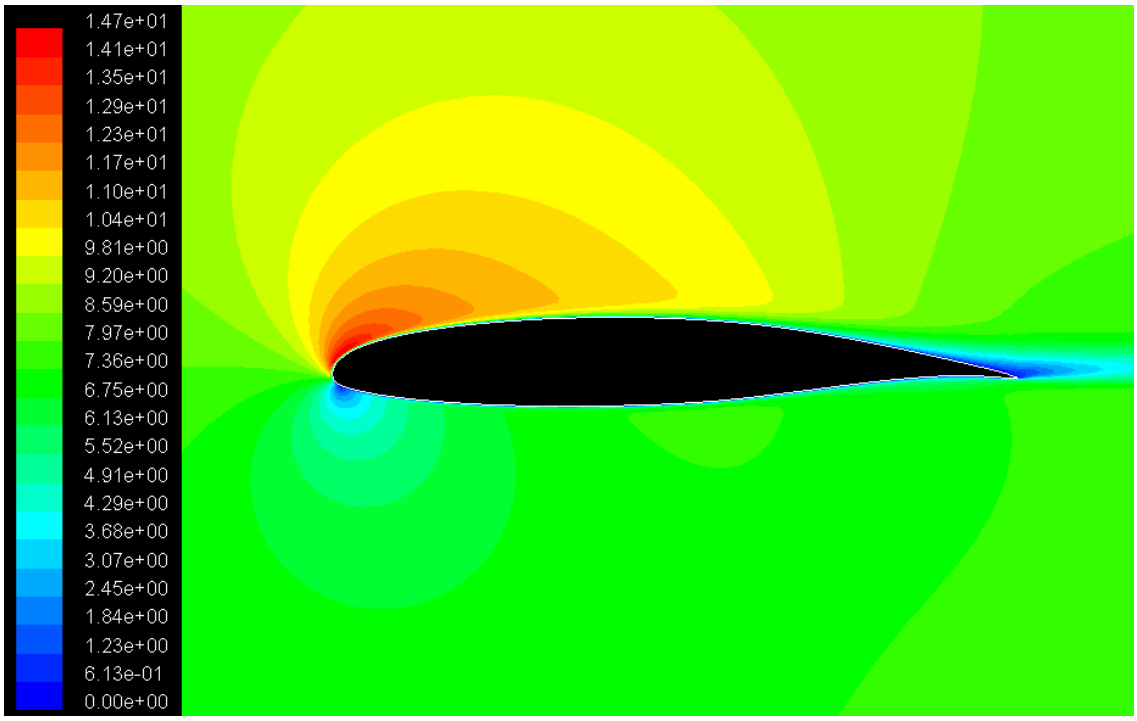

Figure 7.7. Velocity magnitudes for LS(1)413 at $\alpha=8^0$ and Re=5.5e05.

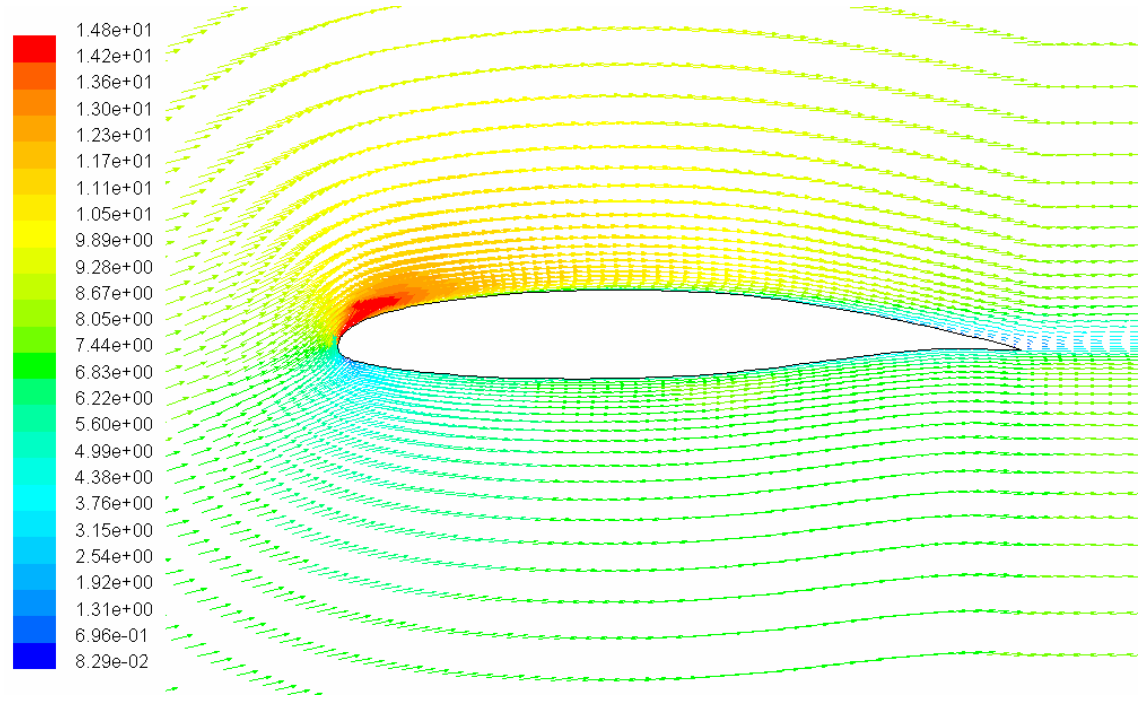

Figure 7.8. Velocity vectors for LS(1)413 at $\alpha=8^0$ and Re=5.5e05.

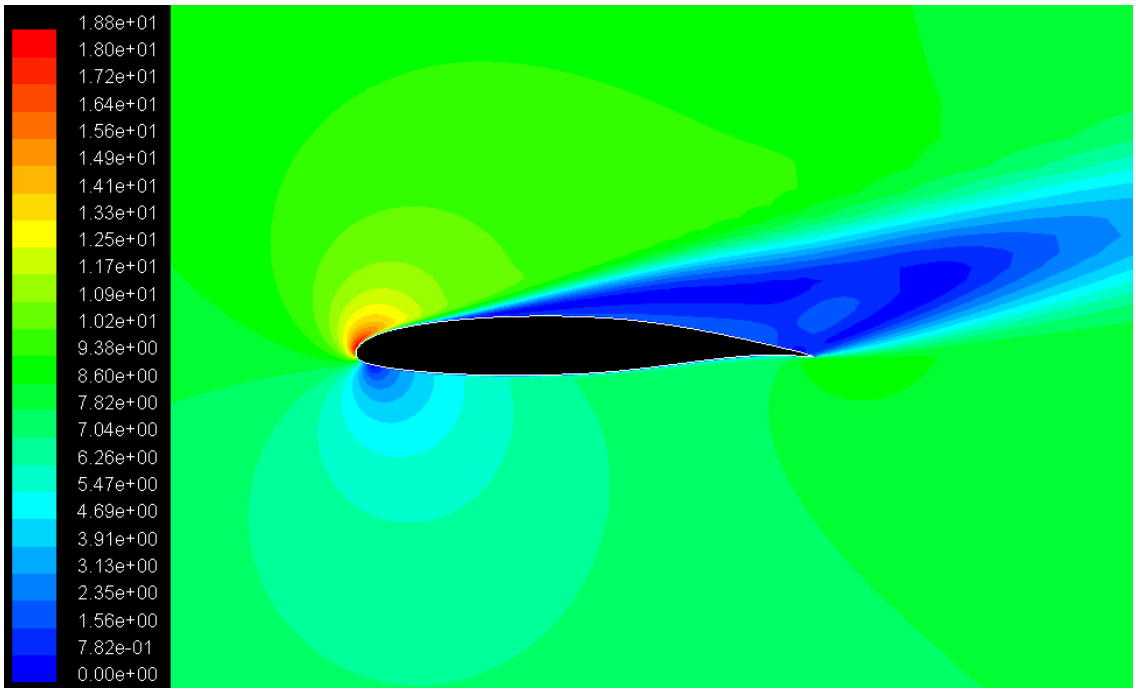

Figure 7.9. Velocity magnitudes for LS(1)413 at $\alpha=18^0$ and Re=5.5e05.

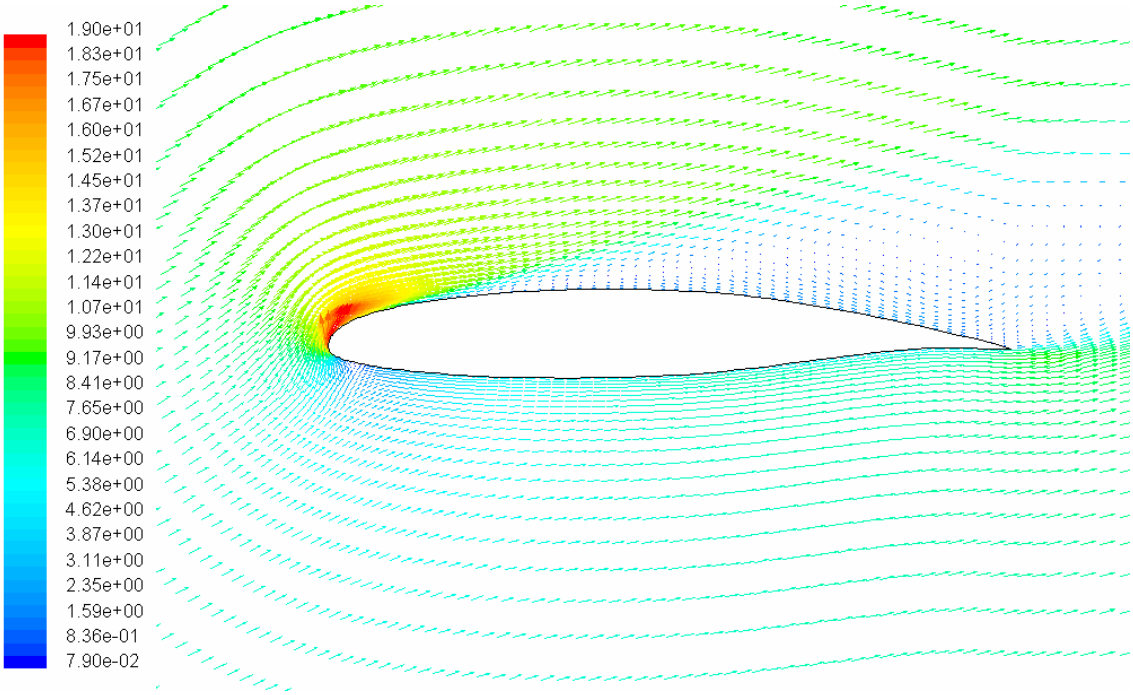

Figure 7.10. Velocity vectors for LS(1)413 at $\alpha=18^0$ and Re=5.5e05.

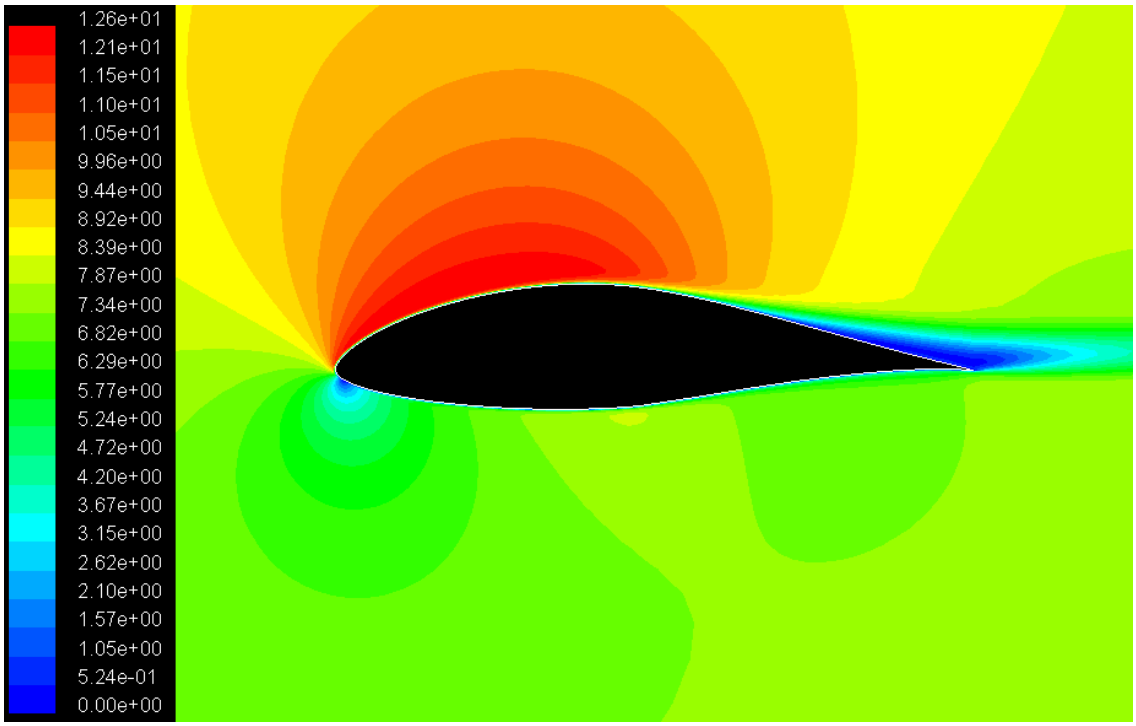

Figure 7.11. Velocity magnitudes for FX66-S196 at $\alpha=8^0$ and Re=5.5e05.

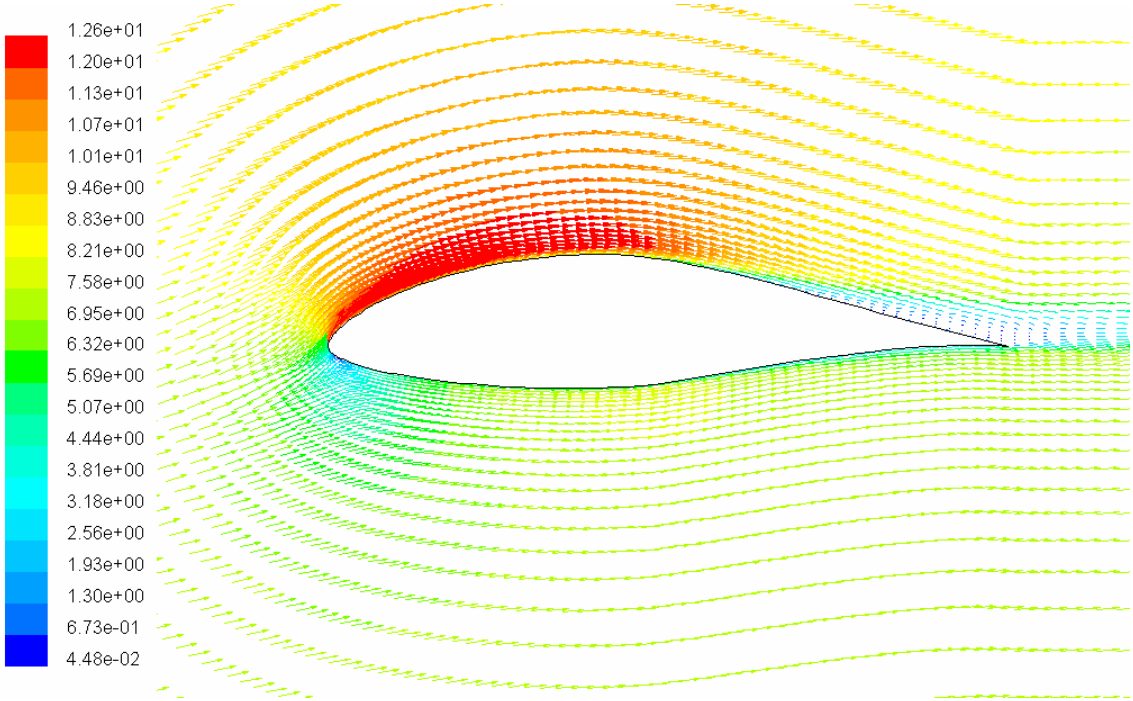

Figure 7.12. Velocity vectors for FX66-S196 at $\alpha=8^0$ and Re=5.5e05.

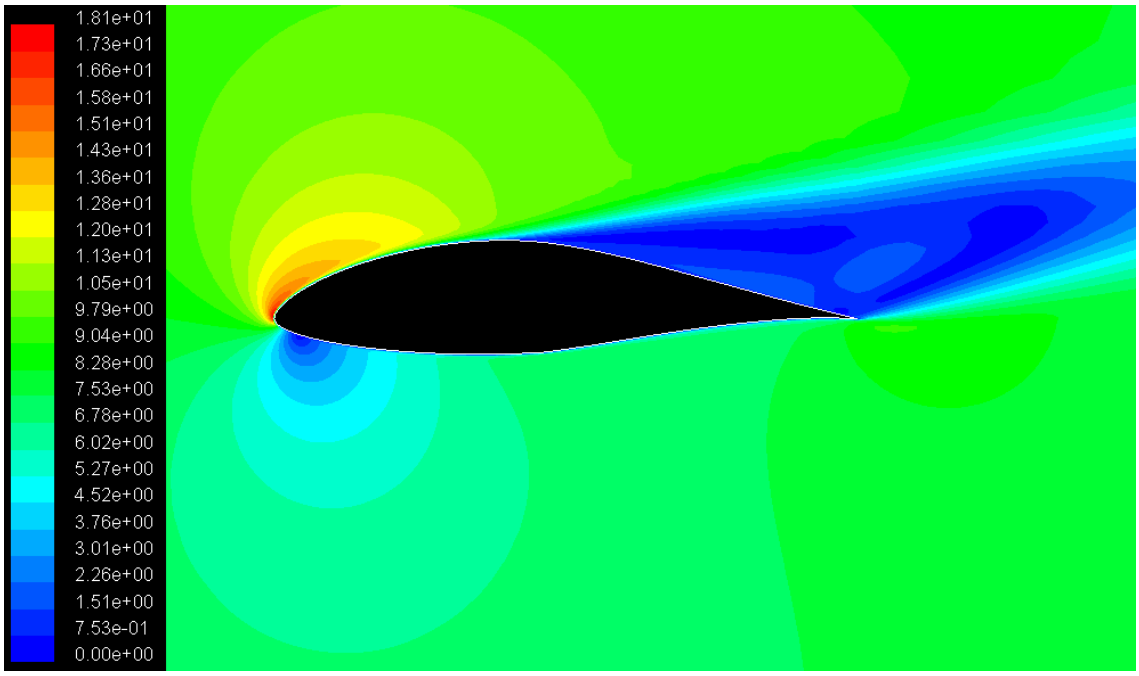

Figure 7.13. Velocity magnitudes for FX66-S196 at $\alpha=18^0$ and Re=5.5e05.

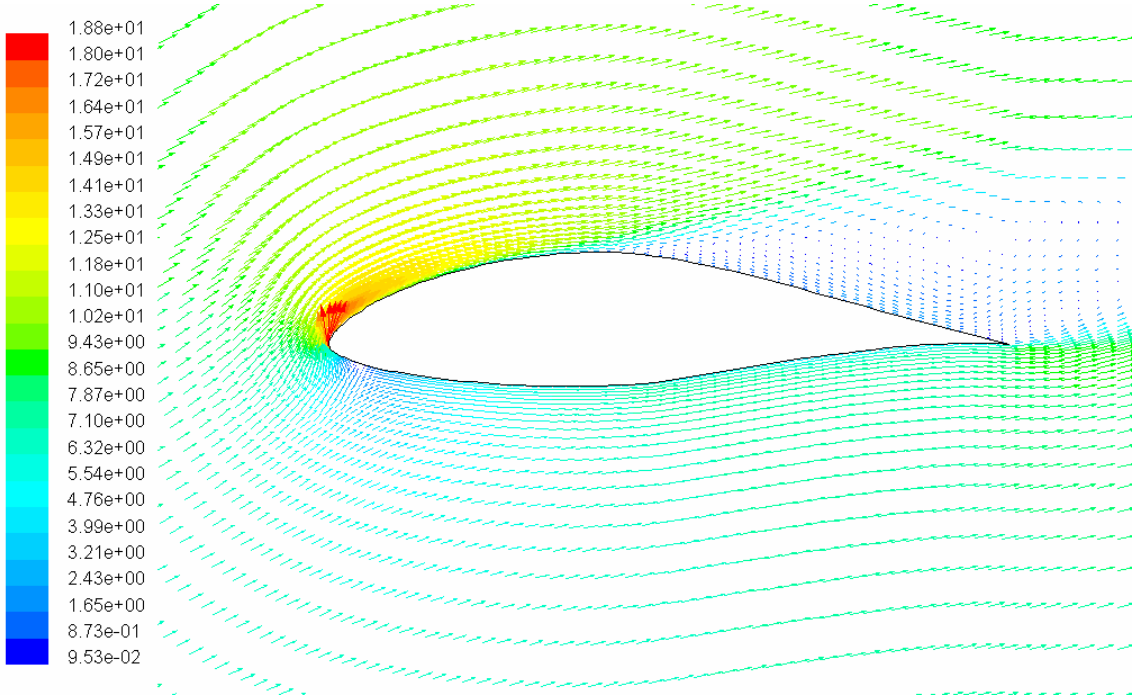

Figure 7.14. Velocity vectors for FX66-S196 at $\alpha=18^0$ and Re=5.5e05.

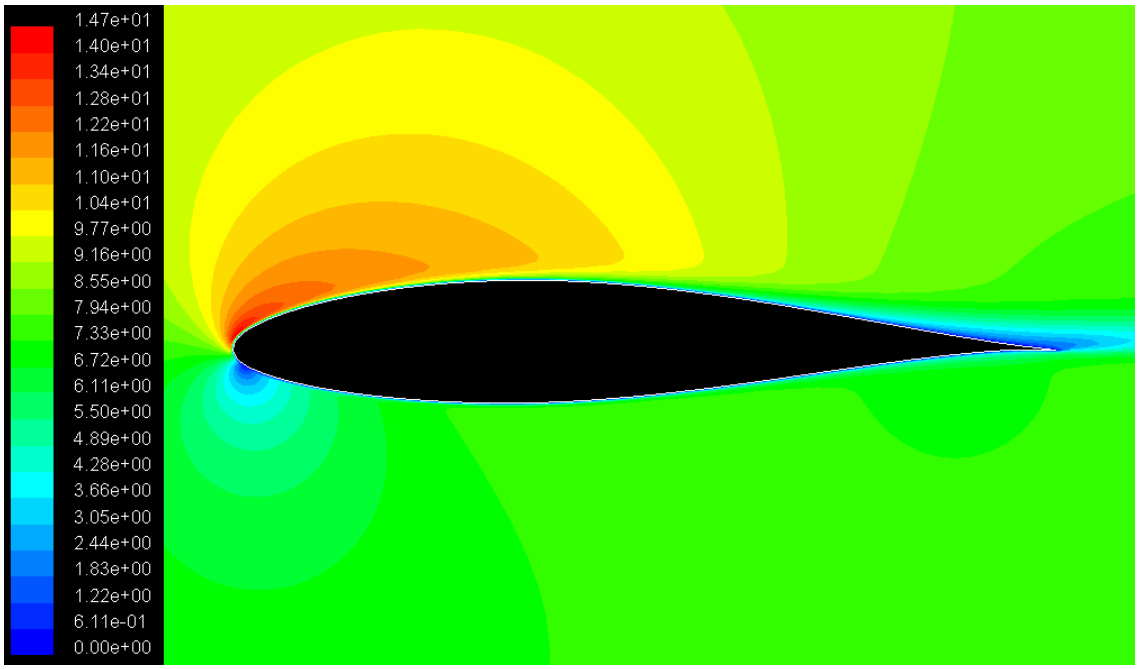

Figure 7.15. Velocity magnitudes for NACA 63215 at $\alpha=8^0$ and Re=5.5e05.

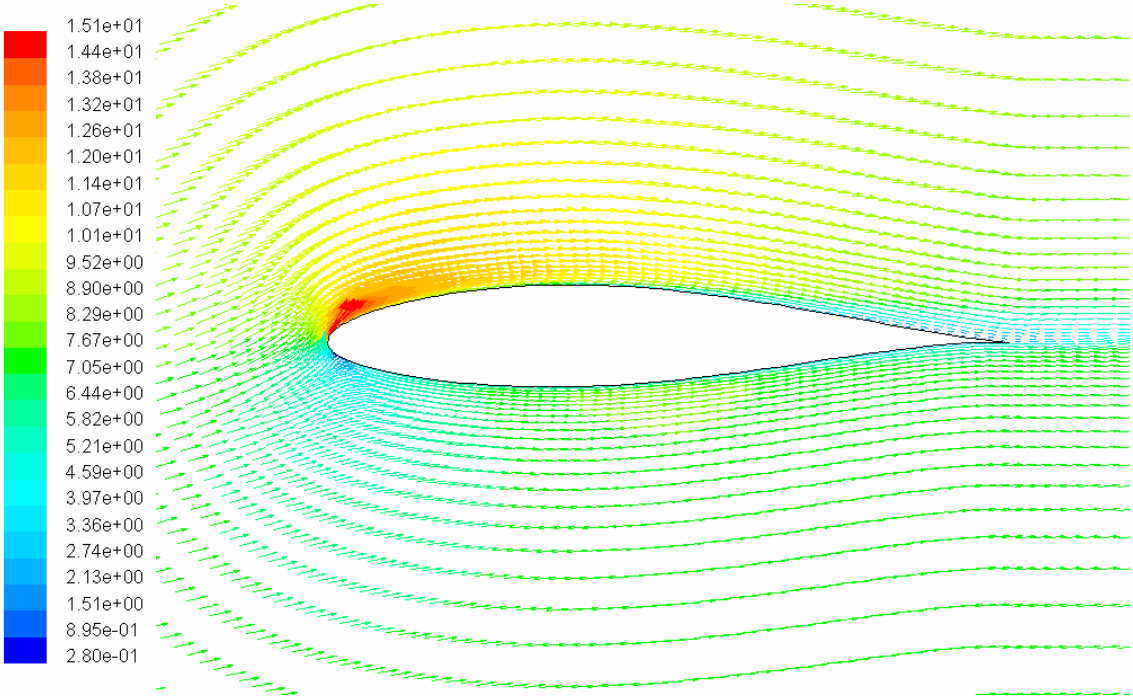

Figure 7.16. Velocity vectors for NACA 63215 at $\alpha=8^0$ and Re=5.5e05.

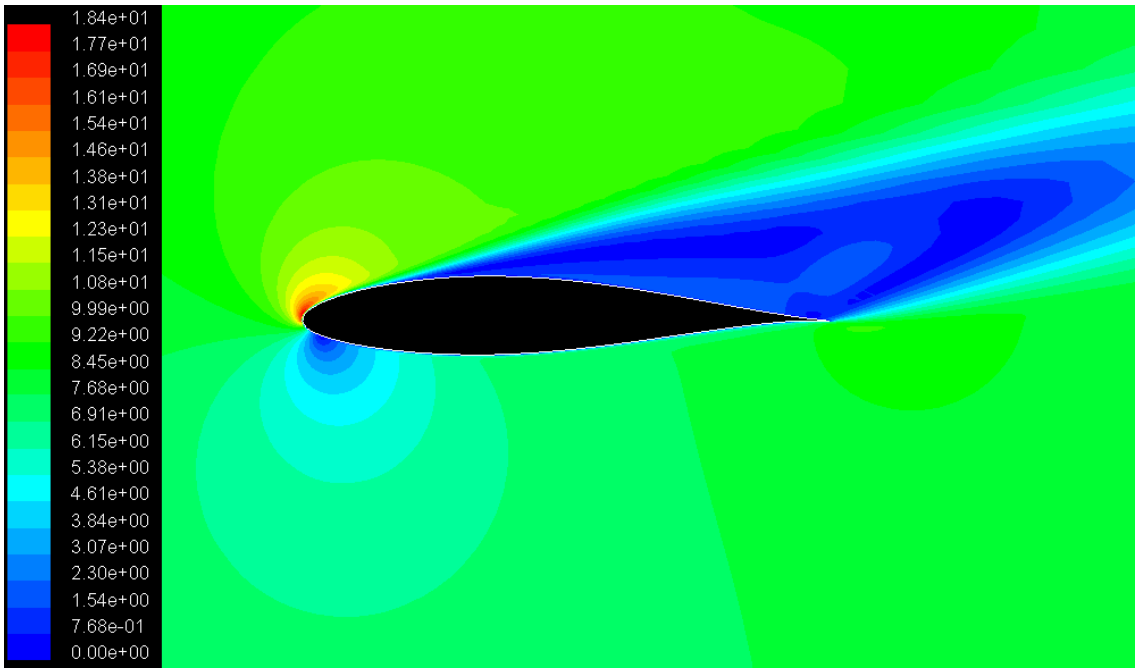

Figure 7.17. Velocity magnitudes for NACA 63215 at $\alpha=18^0$ and Re=5.5e05.

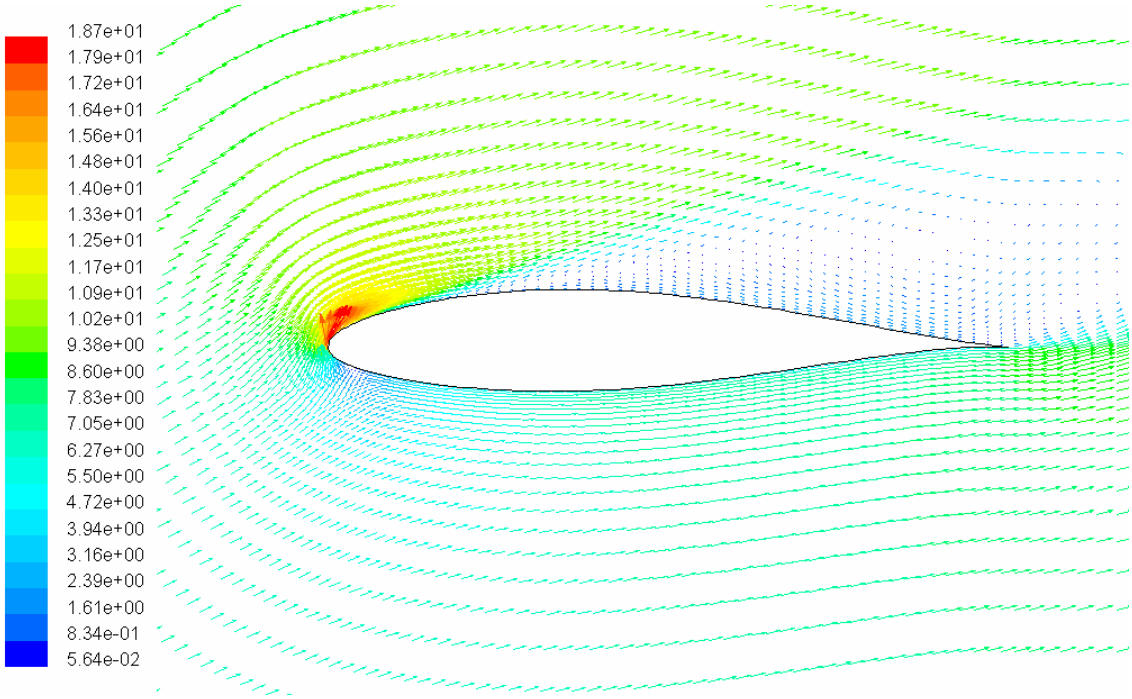

Figure 7.18. Velocity vectors for NACA 63215 at $\alpha=18^0$ and Re=5.5e05.

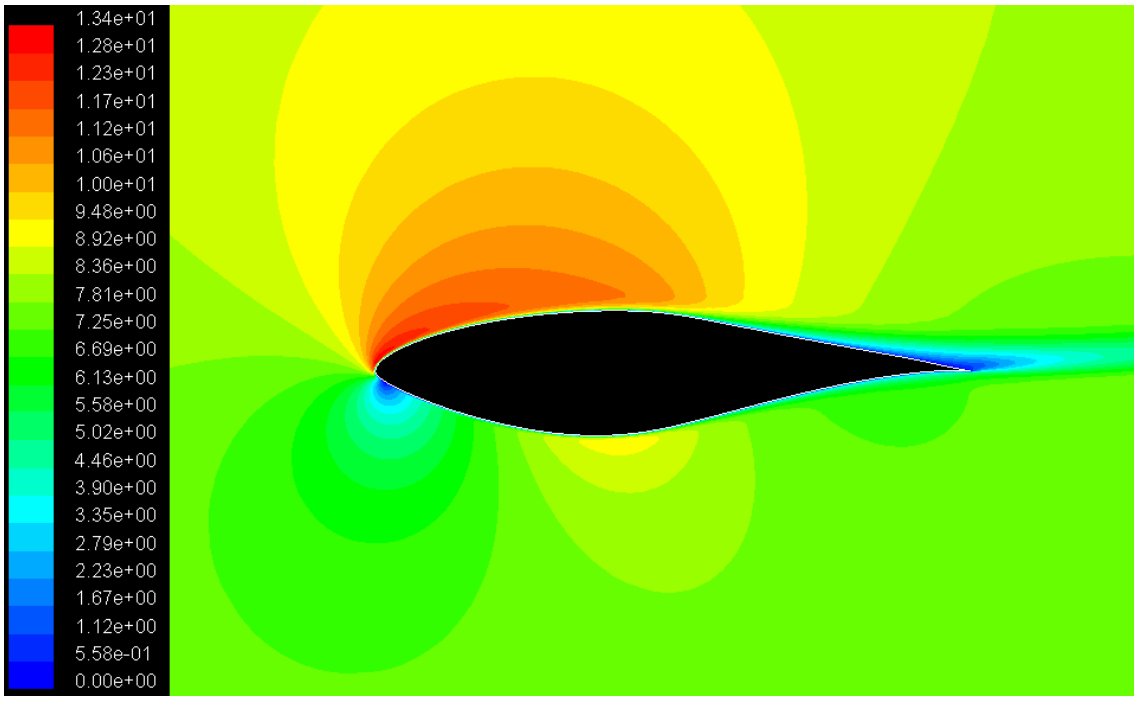

Figure 7.19. Velocity magnitudes for S809 at $\alpha=8^0$ and Re=5.5e05.

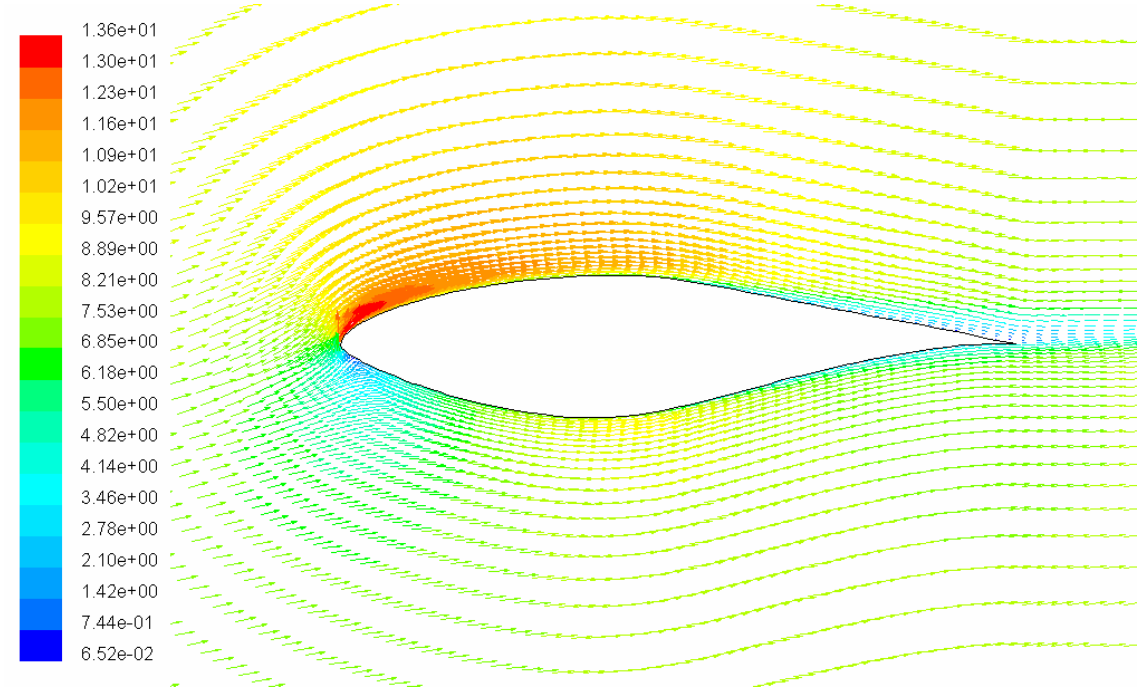

Figure 7.20. Velocity vectors for S809 at $\alpha=8^0$ and Re=5.5e05.

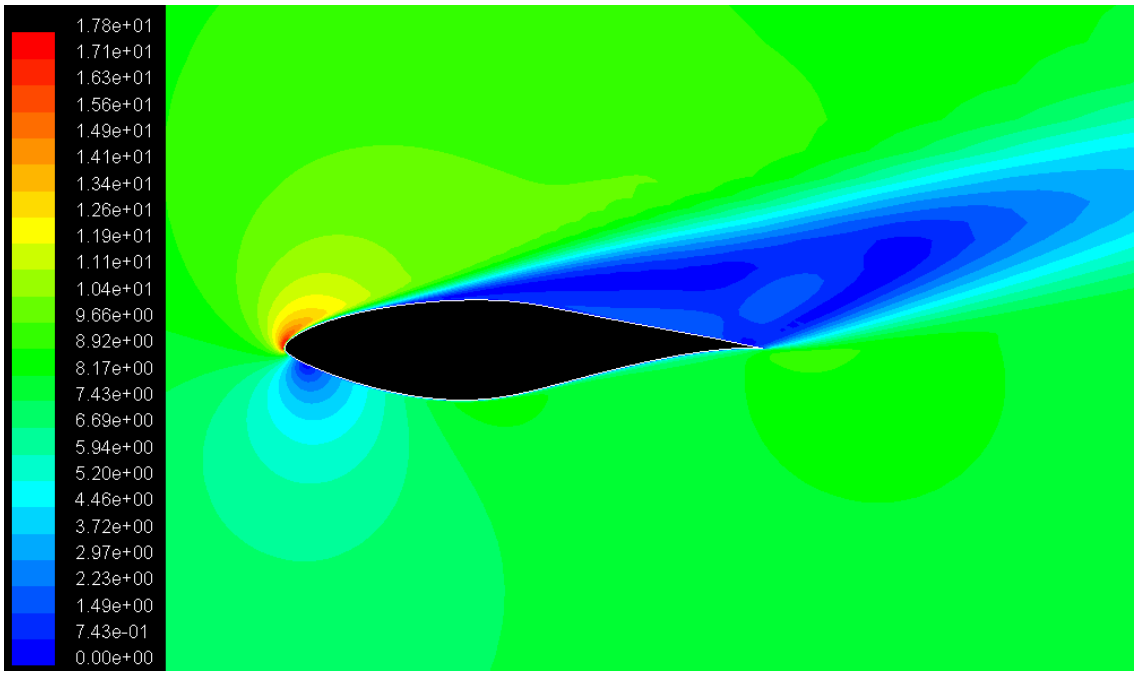

Figure 7.21. Velocity magnitudes for S809 at $\alpha=18^0$ and Re=5.5e05.

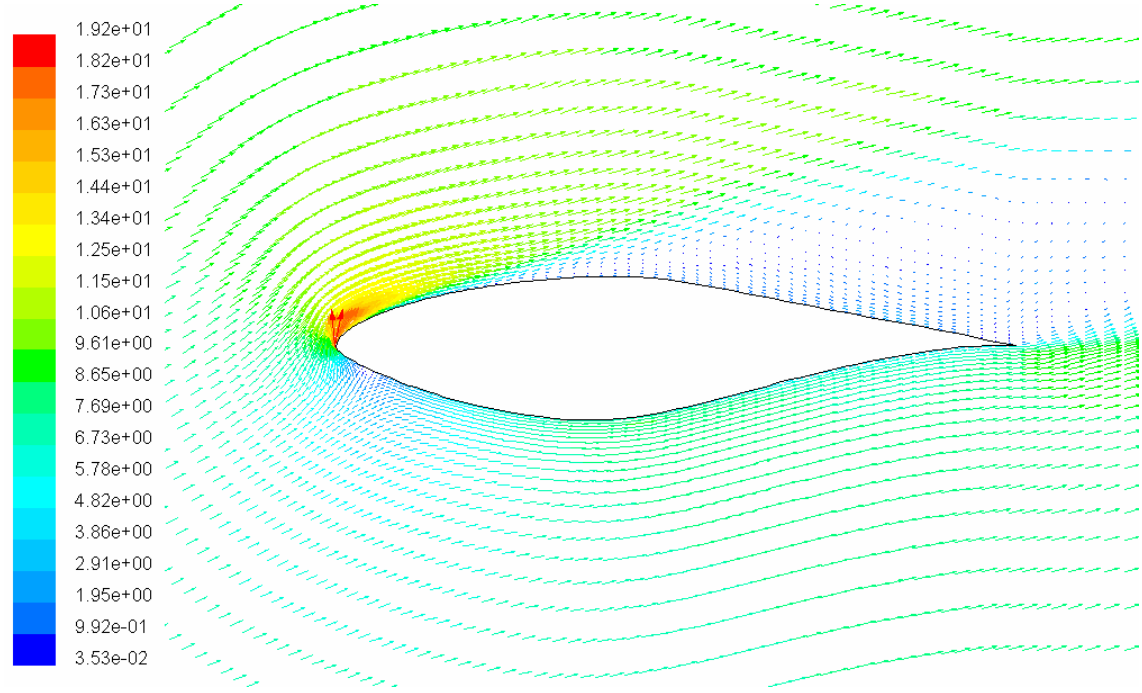

Figure 7.22. Velocity vectors for S809 at $\alpha=18^0$ and Re=5.5e05.

7.2. Tip Speed Ratio, Pitch Angle and Chord Length

Pitch angles are calculated for selected airfoils from Equations 6.2-6. Attack angle is selected as 12^o for LS(1)413 airfoil and 9^o for FX66-S196 airfoil to obtain the power point close to the stall development regime. LS(1)413 airfoil is used up to 0.75 m of rotor. Chord Lengths are calculated from Equation 5.10. Results are shown in Table 7.1.

Table 7.1. Inflow angle, twist angle and chord length distributions along the blade.

r	λ_r	Λ_r	a	a'	θ^+	θ^-	Φ	β	c
0.25	1.051	1.451	0.318	0.168	15.475	44.525	29.050	17.050	0.2150
0.30	1.261	1.610	0.322	0.122	17.197	42.803	25.607	13.607	0.1914
0.35	1.471	1.779	0.324	0.093	18.600	41.400	22.800	10.800	0.1716
0.40	1.682	1.956	0.326	0.072	19.754	40.246	20.492	8.492	0.1550
0.45	1.892	2.140	0.327	0.058	20.713	39.287	18.574	6.574	0.1411
0.50	2.102	2.328	0.328	0.048	21.519	38.481	16.961	4.961	0.1292
0.55	2.312	2.519	0.329	0.040	22.204	37.796	15.592	3.592	0.1190
0.60	2.522	2.713	0.330	0.034	22.792	37.208	14.417	2.417	0.1103
0.65	2.733	2.910	0.330	0.029	23.300	36.700	13.400	1.400	0.1026
0.70	2.943	3.108	0.331	0.025	23.744	36.256	12.512	0.512	0.0959
0.75	3.153	3.308	0.331	0.022	24.134	35.866	11.731	0.269	0.0943
0.80	3.363	3.509	0.331	0.019	24.480	35.520	11.039	2.039	0.0937
0.85	3.573	3.711	0.331	0.017	24.789	35.211	10.423	1.423	0.0924
0.90	3.784	3.914	0.332	0.015	25.065	34.935	9.870	0.870	0.0876
0.95	3.994	4.117	0.332	0.014	25.314	34.686	9.371	0.371	0.0832
1.00	4.204	4.321	0.332	0.012	25.540	34.460	8.920	-0.080	0.0792
1.05	4.414	4.526	0.332	0.011	25.745	34.255	8.509	-0.491	0.0756
1.10	4.624	4.731	0.332	0.010	25.933	34.067	8.135	-0.865	0.0723
1.15	4.835	4.937	0.332	0.009	26.105	33.895	7.791	-1.209	0.0693
1.20	5.045	5.143	0.332	0.009	26.263	33.737	7.475	-1.525	0.0665
1.25	5.255	5.349	0.332	0.008	26.409	33.591	7.183	-1.817	0.0639
1.30	5.465	5.556	0.333	0.007	26.544	33.456	6.913	-2.087	0.0615
1.35	5.676	5.763	0.333	0.007	26.669	33.331	6.662	-2.338	0.0593
1.40	5.886	5.970	0.333	0.006	26.786	33.214	6.428	-2.572	0.0572

7.3. Blade Performance Calculations

Calculations are made for different angular velocities from 200 rpm to 300 rpm. For these angular velocities power, power coefficients and blade element momentum results are obtained. Power results for design conditions are given in Figures 7.15 and 7.16. Effect of twist angle on power coefficients is obtained by calculating same design without twist angles shown in Figure 7.17. At low wind speeds (high tip speed ratios) up to 10 m/s WTPERF is reported having a good agreement with measured power by Tangler. After 10 m/s wind speed over-prediction about 25% is reported (Tangler 2002).

Power characteristics of WH80 and designed rotor for different angular velocities are shown in Figures 7.18 and 7.19 respectively.

Energy production, for designed rotor and rotor in use is calculated with theoretical results for measured wind speeds between July 2000 and July 2001 at 10 meter hub height and angular velocity of 275 rpm. Wind speed frequencies are reported for wind speed values and expected energy values are calculated for these values, results are shown in Table 7.2. Designed rotor gives 5160.5 kWh/year and design in use gives 3482.4 kWh/year. Energy production of designed rotor gives 48.18 % higher values for operating wind speed up to 25 m/s.

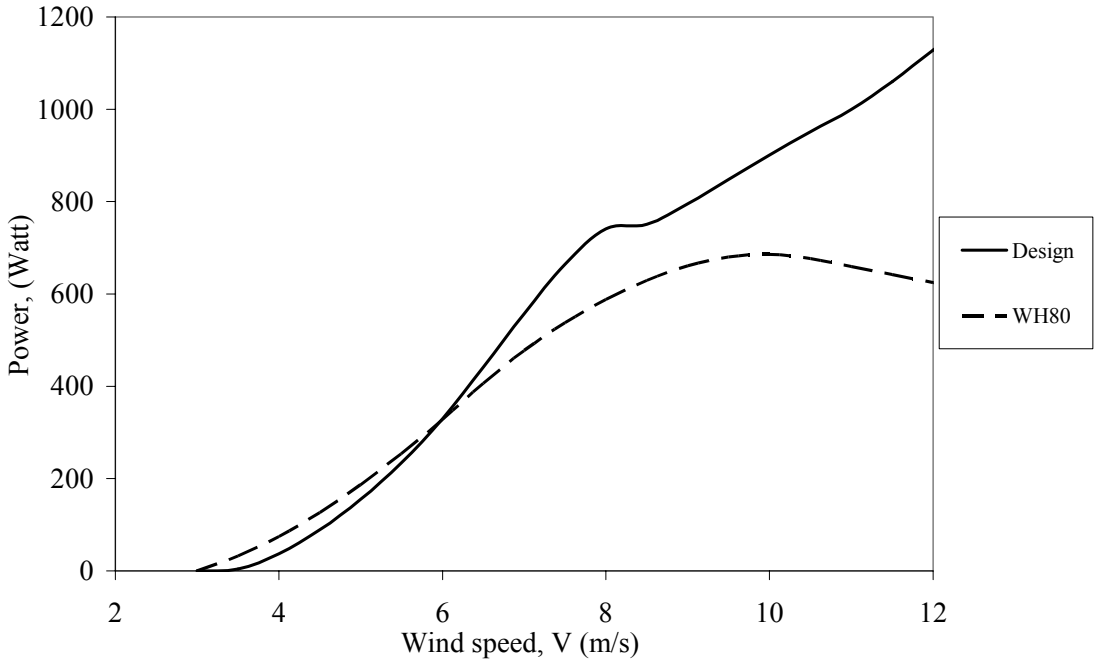

Figure 7.23. Power curves for 275 rpm.

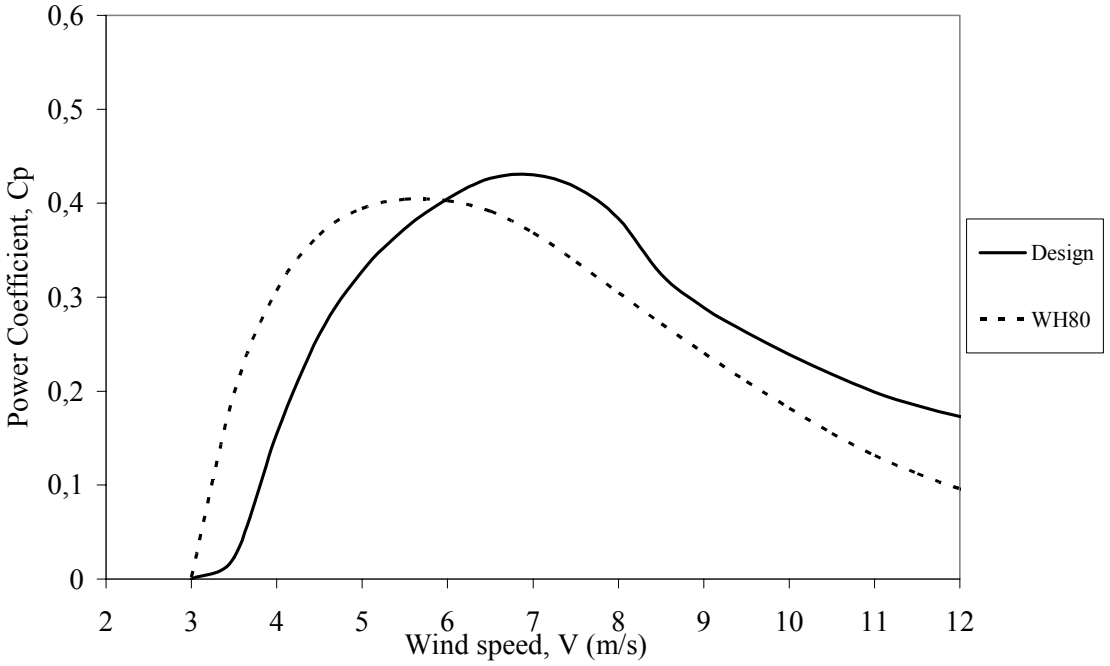

Figure 7.24. Power coefficient curves for 275 rpm

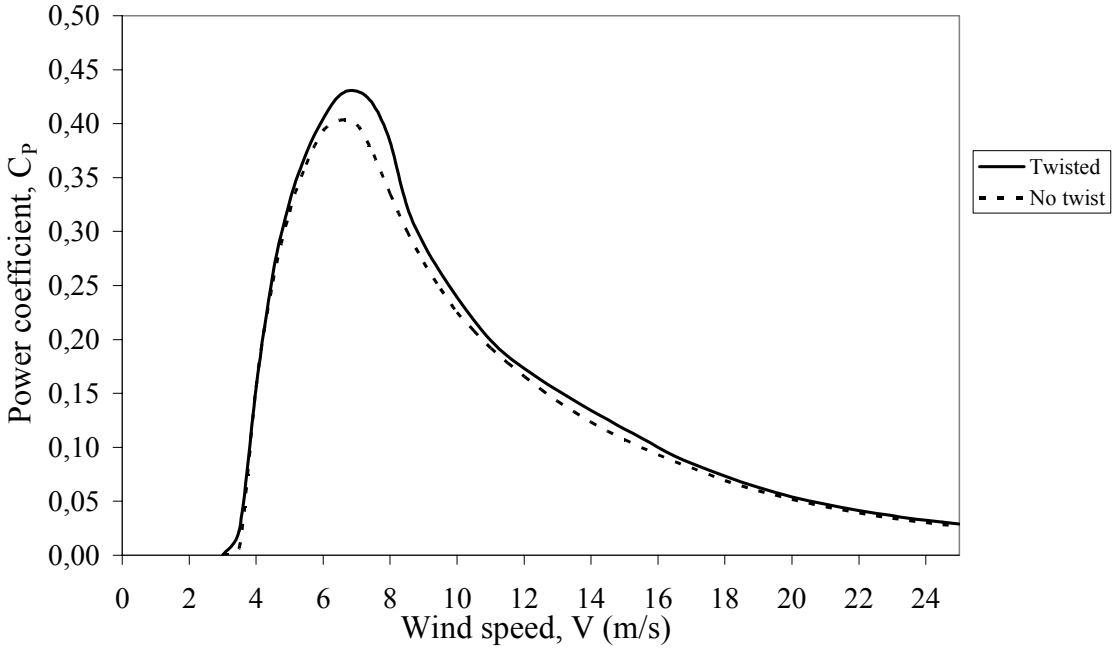

Figure 7.25. Power coefficient curves for designed blade at 275 rpm

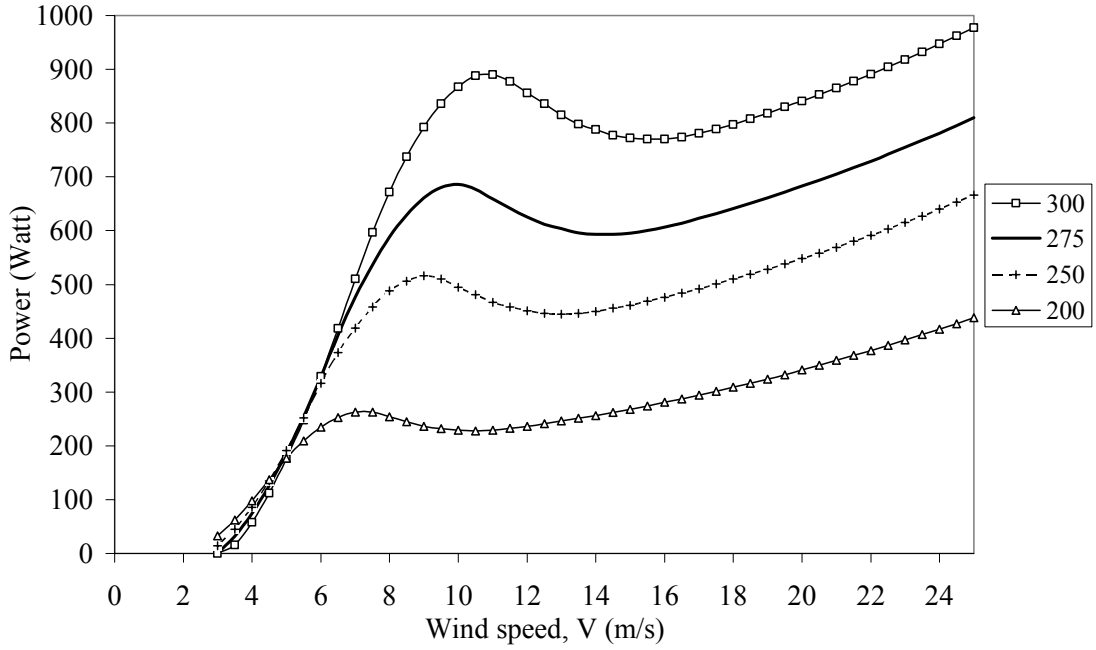

Figure 7.26. WH80 power characteristics for different angular velocities (rpm).

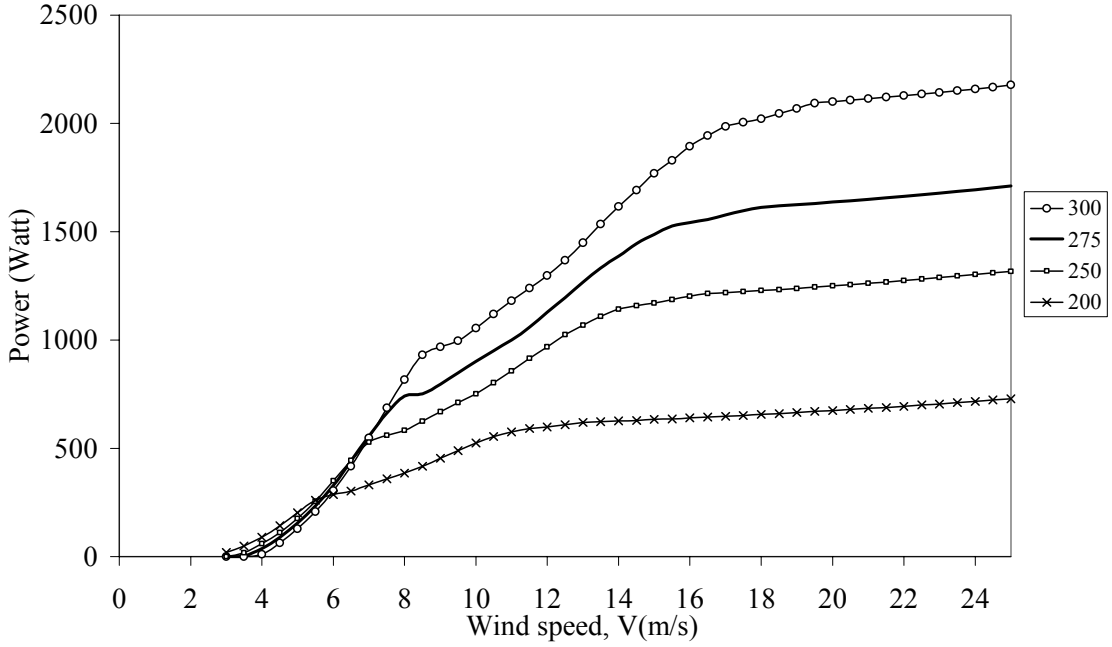

Figure 7.27. Designed rotor power characteristics for different angular velocities (rpm).

Table 7.2. Energy production calculations.

Measurements		Rotor Power (Watt)		Energy Production (kWh)	
Wind Speed (m/s)	Period (min)	New Design	Design in Use	New Design	Design in Use
2.5-3.49	47590	4	10	3.173	7.932
3.5-4.49	50110	43	77	36.191	64.586
4.5-5.49	50430	159	189	133.920	158.574
5.5-6.49	45760	335	329	255.748	251,172
6.5-7.49	44360	554	473	409.837	349.951
7.5-8.49	42030	719	585	503.426	409.559
8.5-9.49	41700	798	657	554.610	456.383
9.5-10.49	39730	900	681	595.950	450.936
10.5-11.49	33900	1004	659	567.072	372.523
11.5-12.49	26550	1128	626	499.140	277.153
12.5-13.49	19790	1265	604	417.349	199.219
13.5-14.49	13780	1388	594	318.854	136.422
14.5-15.49	9720	1486	596	240.786	96.552
15.5-16.49	7090	1542	607	182.252	71.727
16.5-17.49	5880	1577	623	154.546	61.054
17.5-18.49	3730	1610	641	100.068	39.870
18.5-19.49	2910	1625	661	78.813	32.075
19.5-20.49	1730	1637	683	47.200	19.693
20.5-21.49	870	1649	705	23.915	10.227
21.5-22.49	700	1663	729	19.406	8.509
22.5-23.49	390	1678	755	10.909	4.908
23.5-24.49	260	1694	781	7.341	3.386
			Total (kWh/year):	5160.50	3482.41

CHAPTER 8

CONCLUSIONS

In this study, a wind turbine rotor is designed according to the aerodynamic effects on wind turbine blade.

By the use of a software, aerodynamic properties for different airfoils are determined. It is observed that, LS(1)413 gives higher lift coefficients than others for higher angle of attack, Figure 7.5, however its drag coefficient increases dramatically (Figure 7.6). FX66-S196 has got higher and stable lift coefficients at post stall regime (Figure 7.5). It is also seen that there is a smooth increase in drag coefficient of FX66-S196 with increase of angle of attack.

FX66S-196 has got a better transition point location than others (Figures 7.9, 7.13, 7.17, 7.21), separation stops at nearly 0.4c rear from leading edge at $\alpha=18^{o}$ while others' transition point is at about 0.2c rear. As it's known that stall occurs because of the separation and it reduces lift force. So it can be noted that FX66S-196 gives better performance at post stall regime. It can be also noted that numerical code results of airfoil aerodynamics fit better with the newer experimental results.

From these aerodynamic results of airfoils a new blade is designed by selecting the airfoil LS(1)413 for root section and FX66-S196 airfoil for tip section. Chord lengths and twist angles for wind speed at 10 m height in Iztech campus area are optimized with the use of blade element momentum theory. For design wind speed of 6.85 m/s WH80 gives 430 watts with a C_p of 0.3835 and designed blade gives 523 watts with a C_p of 0.4313. WH80 gives highest C_p of 0.4044 at 5.5 m/s wind speed and 254 watts power at this wind speed and angular velocity, where designed rotor gives a power of 234 watts. It is observed that new design gives higher power values than the design in use, over 5.8 m/s wind speed values. It is seen that optimized twist angles increase the power coefficient values. Power coefficient of 0.403 is obtained for designed blade without twist angles (Figure 7.25).

The designed blade enters the stall development regime earlier than the WH80. Because of the design is done, to obtain the work near the stall limit for yielding higher power values without stall at design conditions. Start of the stall is seen from Figure

7.27 that stall delay occurs at about 8 m/s wind speed value.WH80 rotor blade enters stall at about 10 m/s. However designed blade gives higher power values at 10 m/s because of the tip section airfoil of blade. At post stall values, designed wind blade gives higher power values. Because NACA63215 gives lower C_L and higher C_D values than the LS(1)413 and FX66-S196 at these conditions these values are given in Appendix A.

It can be noted that new designed blade is more efficient, as it gives the maximum power coefficient at design conditions of 6.85 m/s wind speed at 10 m height and 25^{o}C ambient temperature.

For further studies a new design can be made for the big scale turbine with a blade pitch control to make turbine blade work near the stall development regime without stall. Also, necessary data for evaluation of rotor blade performance can be produced by conducting experiments.

REFERENCES

Abbott, I.H. and von Doenhoff, A.E., 1959. *Theory of Wing Sections*, (Dover Publications, New York).

Bak, C., Fuglsang, P., Sorensen, N. N., Madsen, H. A., Shen, W.Z., Sorensen, J.N., 1999. *Airfoil Characteristics for Wind Turbines*, (Riso, Roskilde), pp. 7-26.

Bertagnolio, F., Sorensen, N., Johansen, J., Fuglsang, P., 2001. *Wind Turbine Airfoil Catalog*, (Riso, Denmark).

BP, 2005. *Statistical Review of World Energy: Full Report*, (BP),p.4.

Buhl, M.L., 2005. NWTC Design Codes.

El-Wakil, M.M., 1998. *Power Plant Technology*, (McGraw – Hill Book Company, New York), pp. 589-590.

Fluent Incorporated, 1999. *FLUENT 6.1 User's Guide*, (Fluent Incorporated).

Fluent Incorporated, 2003. *FLUENT Training Guide*, (Fluent Incorporated).

Fuglsang, P., Antoniou, I., Sorensen, N.N., Madsen, H.A., 1998. *Validation of a Wind Tunnel Testing Facility for Blade Surface Pressure Measurements*, (Riso, Denmark).

Giguere, P., Selig, M.S., 1999. "Blade Design Trade-Offs Using Low-Lift Airfoils for Stall Regulated HAWT's", (ASME/AIAA Wind Energy Symposium, Nevada), NREL, Colorado.

Golding, E.W., 1977. *The Generation of Electricity by Wind Power*, (E.& F.N. Spon Ltd., London).

Gross, R., Leach, M. and Bauen A., 2003. "Progress in Renewable Energy", *Environment International*. Vol.29, No.1, pp. 105-122.

Habali, S.M. and Saleh, I.A., 2000. "Local design, testing and manufacturing of small mixed airfoil wind turbine blades of glass fiber reinforced plastics- Part I- Design of the blade and root", *Energy Conversion and Management*.Vol.41, No.3, pp. 249-280.

Hatziargyriou, N. and Zervas A., 2001. "Wind Power Development in Europe", *Proceedings of the IEE*. Vol.89, No.12, pp.1765-1782.

Hau, E., 2000. *Wind Turbines, Fundamentals, Technologies, Application, Economics*, (Springer-Verlag, Berlin).

Kaufman, J.W. 1977. "Terrestrial Environment (Climatic) Criteria Guidelines for Use in Aerospace Vehicle Development", (NASA TM X-78118, Huntsville, Alabama).

Lissaman, P.B.S., 1998. “Wind Turbine Airfoils and Rotor Wakes” in *Wind Turbine Technology Fundamental Concepts of Wind Turbine Engineering*, edited by D.A. Spera (ASME New York), pp. 283-321.

Maalawi, K.Y. and Badawy, M.T.S.,2001. “A Direct Method of Evaluating Performance of Horizontal Axis Wind Turbines”, *Renewable and Sustainable Energy Reviews*. Vol.5, pp. 175-190.

Manwell, J., McGowan, J., Rogers, A., 2004. *Wind Energy Explained: Theory, Design and Application* , (Wiley & Sons, New York), pp. 83-134.

Mikkelsen, R., 2003. *Actuator Disc Methods Applied to Wind Turbines*, (DTU, Lyngby, Denmark), pp. 6-24.

Ozerdem, B. and Turkeli, H.M. 2005. “Wind Energy Potential Estimation and Micrositting on Izmir Institute of Technology Campus, Turkey”, *Renewable Energy*. Vol.30, No.10 pp.1623-1633

Shepherd, D., 1998. “Historical Development of Windmill”, in *Wind Turbine Technology Fundamental Concepts of Wind Turbine Engineering*, edited by D.A. Spera (ASME New York), pp. 1-46.

Somers, D.M., 1997. *Design and Experimental Results for the S809 Airfoil*, (NREL, Colorado).

Spera, D.A. and Richards,T.R., 1979. “Modified Power Law Equations for Vertical Wind Profiles”, (NASA TM-79275, DOE/NASA/1059-79/4, Cleveland, Ohio)

Tangler, J.L., 2002. “The Nebulous Art of Using Wind-Tunnel Airfoil Data for Predicting Rotor Performance”, (21st ASME Wind Energy Conference, Nevada), NREL, Colorado.

Tangler, J.L. and Korucek, J.D., 2005. “Wind Turbine Post Stall Airfoil Performance Characteristics Guidelines for Blade Element Momentum Methods”, (43rd AIAA Aerospace Sciences, Nevada), NREL, Colorado.

T.C. Resmi Gazete, 2004, No.25639 Part.3

Walker, J.F. and Jenkins, N., 1997. *Wind Energy Technology*, (Wiley & Sons, New York), p.51.

WEB_1, 2005. European Wind Energy Association, 20/05/2005. http://www.ewea.org/06projects_events/proj_WEfacts.htm

WEB_2, 2005. Global wind Energy Council, 20/05/2005. http://www.gwec.net/fileadmin/documents/PressReleases/0304-GlobalWindEnergyMarkets-FINAL.pdf

WEB_3, 2005. US Department of Energy-Energy Overview of Turkey, http://www.fe.doe.gov/international/South_and_Southwest_Asia/turkover.html

WEB_4, 2005. The world of wind atlases, 12/03/2005. http://www.windatlas.dk/Europe/Index.htm

WEB_5, 2005. Centre for energy, 15/06/2005.
http://www.centreforenergy.com/silos/wind/windEnvironment

WEB_6, 2005. Danish Wind Industry Association,
http://www.windpower.org/en/pictures/

WEB_7, 2005. Dromey Design,
http://www.dromeydesign.com/articles/generators_and_motors.htm

Wilson, P.E., 1998. "Aerodynamic Behavior of Wind Turbines" in *Wind Turbine Technology Fundamental Concepts of Wind Turbine Engineering*, edited by D.A. Spera (ASME New York), pp. 215-282.

APPENDIX A

VITERNA CALCULATIONS OF AIRFOILS

	FX66-S196		LS(1)413		NACA 63215	
α	C_L	C_D	C_L	C_D	C_L	C_D
-180	0,0000	0,0100	0	0,0618999	0	0,0729682
-170	0,4473	0,0100	0,4166441	0,0998578	0,3675665	0,1107579
-160	0,8945	0,0476	0,8332882	0,2090682	0,735133	0,219469
-150	0,8292	0,2273	0,7065304	0,3761069	0,6495029	0,3856923
-140	0,7113	0,4488	0,6366737	0,580415	0,6019654	0,5888938
-130	0,6022	0,6863	0,5580939	0,7967916	0,5375882	0,8039061
-120	0,4753	0,9125	0,4517323	0,99845	0,4407574	1,0039841
-110	0,3266	1,1015	0,3164036	1,1602697	0,3116709	1,1640553
-100	0,1634	1,2320	0,1608627	1,2618505	0,1596986	1,2637725
-90	0,0000	1,2900	-5,529E-17	1,29	-5,529E-17	1,29
-80	-0,1634	1,2320	-0,1608627	1,2618505	-0,1596986	1,2637725
-70	-0,3266	1,1015	-0,3164036	1,1602697	-0,3116709	1,1640553
-60	-0,4753	0,9125	-0,4517323	0,99845	-0,4407574	1,0039841
-50	-0,6022	0,6863	-0,5580939	0,7967916	-0,5375882	0,8039061
-40	-0,7113	0,4488	-0,6366737	0,580415	-0,6019654	0,5888938
-30	-0,8292	0,2273	-0,7065304	0,3761069	-0,6495029	0,3856923
-20	-0,8646	0,0732	-0,8332882	0,2090682	-0,735133	0,219469
-10	-0,2678	0,0440	-0,280446	0,1113968	-0,3065283	0,1143662
0	0,4701	0,0147	0,3891375	0,0137254	0,174395	0,0092635
2	0,6863	0,0160	0,5831324	0,0161429	0,4039	0,00995
4	0,8927	0,0183	0,8089712	0,0175458	0,6289	0,01128
6	1,0884	0,0212	0,9977228	0,0210803	0,85046	0,01325
8	1,2474	0,0264	1,1708857	0,0262772	1,05946	0,01661
10	1,3376	0,0367	1,3138438	0,0335352	1,24848	0,02184
12	1,3630	0,0537	1,4266792	0,0435997	1,3823	0,03099
14	1,4044	0,0786	1,4954451	0,0586028	1,3593	0,056127
15	1,3985	0,0845	1,5147252	0,0581797	1,2812	0,07843
16	1,3900	0,0938	1,4916949	0,0718778	1,20207	0,106106
18	1,4205	0,1219	1,329042	0,1351394	1,08766	0,16563
20	1,4007	0,1535	1,1904117	0,2090682	1,05019	0,219469
30	1,1845	0,2273	1,0093291	0,3761069	0,9278612	0,3856923
40	1,0162	0,4488	0,9095339	0,580415	0,8599506	0,5888938
50	0,8603	0,6863	0,7972769	0,7967916	0,7679831	0,8039061
60	0,6791	0,9125	0,6453319	0,99845	0,6296534	1,0039841
70	0,4665	1,1015	0,4520052	1,1602697	0,4452442	1,1640553
80	0,2334	1,2320	0,2298038	1,2618505	0,2281408	1,2637725
90	0,0000	1,2900	7,899E-17	1,29	7,899E-17	1,29

100	-0,1634	1,2320	-0,1608627	1,2618505	-0,1596986	1,2637725
110	-0,3266	1,1015	-0,3164036	1,1602697	-0,3116709	1,1640553
120	-0,4753	0,9125	-0,4517323	0,99845	-0,4407574	1,0039841
130	-0,6022	0,6863	-0,5580939	0,7967916	-0,5375882	0,8039061
140	-0,7113	0,4488	-0,6366737	0,580415	-0,6019654	0,5888938
150	-0,8292	0,2273	-0,7065304	0,3761069	-0,6495029	0,3856923
160	-0,8945	0,0476	-0,8332882	0,2090682	-0,735133	0,219469
170	-0,4473	0,0100	-0,4166441	0,0998578	-0,3675665	0,1107579
180	0,0000	0,0100	0	0,0618999	0	0,0729682